AD-762 443

STUDIES OF WAVE AND FRACTURE PROPAGATION IN ROCK MEDIA

I. M. Daniel, et al

IIT Research Institute

Prepared for:

Bureau of Mines

June 1973

IITRI

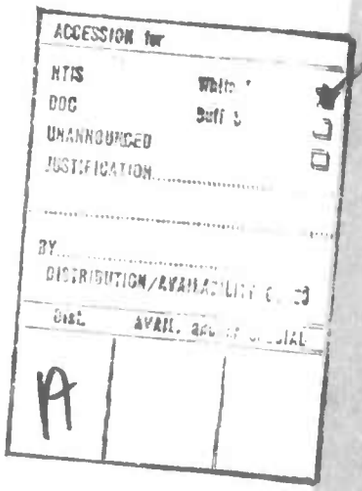

Advanced concepts are being used by IIT Research Institute to solve research, development, and design problems for industry and government through contract research. Our services encompass virtually all of the physical and biological sciences. Principal areas are: chemistry, computer sciences, electronics, engineering mechanics, life sciences, mechanics of materials, medical engineering, metals, and management and social science research.

The interdisciplinary approach at IITRI brings the latest technology to bear upon the problem-solving process.

Principal office:
10 West 35th Street
Chicago, Illinois 60616

IITRI Research Project No. D6069

(Final Report)

STUDIES OF WAVE AND FRACTURE PROPAGATION IN ROCK MEDIA

for

Bureau of Mines
U. S. Department of the Interior
Twin Cities, Minnesota

June 1973

Security Classification

DOCUMENT CONTROL DATA - R & D

(Security classification of title, body of abstract and indexing annotation must be entered when the overall report is classified)

1. ORIGINATING ACTIVITY (Corporate author) IIT Research Institute, Technology Ctr. Chicago, Illinois 60616	2a. REPORT SECURITY CLASSIFICATION Unclassified 2b. GROUP

3. REPORT TITLE

STUDIES OF WAVE AND FRACTURE PROPAGATION IN ROCK MEDIA

4. DESCRIPTIVE NOTES (Type of report and inclusive dates)
Final Report, 3 February 1972 to 2 March 1973

5. AUTHOR(S) (First name, middle initial, last name)

I. M. Daniel and R. E. Rowlands

6. REPORT DATE June 1973	7a. TOTAL NO. OF PAGES 89	7b. NO. OF REFS 29
8a. CONTRACT OR GRANT NO. H0220024 b. PROJECT NO. ARPA Order No. 1579 c. Amendment No. 3 d. Program Code 2F10	9a. ORIGINATOR'S REPORT NUMBER(S) 9b. OTHER REPORT NO(S) (Any other numbers that may be assigned this report) IITRI Report D6069	

10. DISTRIBUTION STATEMENT

Distribution of this document is unlimited.

11. SUPPLEMENTARY NOTES	12. SPONSORING MILITARY ACTIVITY

Details of illustrations in this document may be better studied on microfiche.

13. ABSTRACT

Experimental stress analysis techniques were used to study wave and fracture propagation in rock and rocklike media. Transparent birefringent specimens of CR-39, Plexiglas and Homalite-100 were loaded with explosive charges and isochromatic fringe patterns and crack propagation were recorded with a multiple spark camera operating at a rate of 200,000 frames per second. Dilatational wave, shear wave and crack propagation velocities were measured. In the case of CR-39 crack velocities were measured up to half the shear wave velocity, which represents the theoretical limit velocity. Marble and granite plates were loaded explosively and isochromatic fringe patterns on bonded photoelastic coatings and moiré fringe patterns were recorded with a Beckman and Whitley camera operating at rates from 250,000 to 1,000,000 frames per second. Dilatational, shear and Rayleigh wave velocities were measured. The leading part of the pulse is compressive and shows appreciable attenuation. The trailing part goes into tension causing widespread tensile fracture. The velocity of propagation of this fracture zone in marble was nearly equal the theoretical terminal velocity. In the case of induced cracks in marble and granite, the velocities of crack propagation

DD FORM 1 NOV 65 1473

Security Classification

ABSTRACT (Cont'd.)

DD Form 1473

were appreciably lower than the theoretical terminal values. Experimental results obtained were discussed and interpreted for their relevance to the rapid excavation process in rock.

Security Classification

14. KEY WORDS	LINK A		LINK B		LINK C	
	ROLE	WT	ROLE	WT	ROLE	WT
Wave Propagation						
Crack Propagation						
Rock Mechanics						
Dynamic Photoelasticity						
Dynamic Moiré						
Photoelastic Coatings						
High-Speed Photography						
Rapid Excavation						
Explosive Excavation						

Security Classification

IIT RESEARCH INSTITUTE
Technology Center
Chicago, Illinois 60616

IITRI Project No. D6069

Final Report

STUDIES OF WAVE AND FRACTURE PROPAGATION IN ROCK MEDIA

by

I. M. Daniel
R. E. Rowlands

Monitored by

Bureau of Mines
U. S. Department of the Interior
Twin Cities, Minnesota

Sponsored by

Advanced Research Projects Agency
Arlington, Virginia

June 1973

ia

IITRI Project No. D6069
Final Report
February 3, 1972 to February 2, 1973

Sponsored by:
Advanced Research Projects Agency

ARPA Order: No. 1579, Amend. No. 3

Program Code: 2F10

Name of Contractor: IIT Research Institute
10 West 35th Street
Chicago, Illinois 60616

Effective Date of Contract: 3 February 1972

Contract Expiration Date: 2 March 1973

Amount of Contract: $47,626

Contract Number: H0220024

Principal Investigator and Phone Number:

Isaac M. Daniel
312/225-9630, extension 4773

Project Engineer and Phone Number:

Robert E. Rowlands
312/225-9630, extension 5350

Title of Work: "Studies of Wave and Fracture Propagation in Rock Media"

FOREWORD

This is the final report on IIT Research Institute (IITRI) Project No. D6069, "Studies of Wave and Fracture Propagation in Rock Media," describing research work conducted in the period between 3 February 1972 and 2 February 1973. The program was conducted under Contract No. H0220024 with the Bureau of Mines of the U. S. Department of the Interior, with Mr. Joseph L. Condon of the Twin Cities Mining Research Center acting as project officer. The program was conducted at IITRI with Dr. I. M. Daniel as principal investigator and Dr. R. E. Rowlands as project engineer. Other IITRI staff contributing to the program include Messrs. J. E. Daley, R. P. Joyce, R. R. King, T. Niiro and J. Smith.

Respectfully submitted,
IIT RESEARCH INSTITUTE

I. M. Daniel
Manager
Stress Analysis

APPROVED:

R. H. Cornish
Director of Research
Mechanics of Materials Division

IMD:jm

STUDIES OF WAVE AND FRACTURE PROPAGATION IN ROCK MEDIA

ABSTRACT

Experimental stress analysis techniques were used to study wave and fracture propagation in rock and rocklike media. Transparent birefringent specimens of CR-39, Plexiglas and Homalite-100 were loaded with explosive charges and isochromatic fringe patterns and crack propagation were recorded with a multiple spark camera operating at a rate of 200,000 frames per second. Dilatational wave, shear wave and crack propagation velocities were measured. In the case of CR-39 crack velocities were measured up to half the shear wave velocity, which represents the theoretical limit velocity. Marble and granite plates were loaded explosively and isochromatic fringe patterns on bonded photoelastic coatings and moiré fringe patterns were recorded with a Beckman and Whitley camera operating at rates from 250,000 to 1,000,000 frames per second. Dilatational, shear and Rayleigh wave velocities were measured. The leading part of the pulse is compressive and shows appreciable attenuation. The trailing part goes into tension causing widespread tensile fracture. The velocity of propagation of this fracture zone in marble was nearly equal the theoretical terminal velocity. In the case of induced cracks in marble and granite, the velocities of crack propagation were appreciably lower than the theoretical terminal values. Experimental results obtained were discussed and interpreted for their relevance to the rapid excavation process in rock.

CONTENTS

LIST OF ILLUSTRATIONS

LIST OF ILLUSTRATIONS (Cont'd.)

LIST OF ILLUSTRATIONS (Cont'd.)

LIST OF ILLUSTRATIONS (Cont'd.)

STUDIES OF WAVE AND FRACTURE PROPAGATION IN ROCK MEDIA

1.0 INTRODUCTION

The increasing needs for urban and resource development demand faster, safer and more efficient procedures for underground excavation in rock.[1] The technology of underground excavation, especially in hard rock, is not progressing in step with the needs. Advancement of this technology requires knowledge of the geologic conditions in the region of the excavation, i.e., the type of rocks and soil present, and basic rock mechanics, i.e., in-situ rock properties and the state of stress present. The most important process involved in rapid excavation is rock disintegration. The phenomenon of rock fracture and its relationship to the methods of excavation and rock properties is not well understood.

All methods of rapid excavation in hard rock must use some form of dynamic or impact loading on the rock, whether it is by means of an explosive or a water jet. This type of loading produces stress waves which induce and propagate fracture. The whole process of rock breakage then is a complicated interaction of stress wave and crack propagation. The problem of wave propagation in elastic materials is well understood but it has not been adequately studied in the case of rock with its intrinsic properties of inhomogeneity, anisotropy and the presence of discontinuities. The problem of fracture propagation in rock is even more complex than that of stress wave propagation.

To understand better the fracture processes in rock, it is necessary to study its response to dynamic loading. Stress wave propagation and fracture initiation and propagation must be studied and correlated. This requires the measurement and correlation of stress wave velocities, i.e., dilatational, shear and Rayleigh, and the terminal crack propagation velocity.

Analytical approaches are often limited as they cannot fully account for material inhomogeneity, anisotropy, inelasticity and defects. The most promising approach then, is the experimental one. Techniques such as dynamic photoelasticity, photoelastic coatings, moiré and strain gages are very useful and suitable for testing rock and simulated rock specimens.

The objectives of this program are to study wave and crack propagation and their interaction in rock and rock-like media using the experimental techniques above, correlate the results with available theory and interpret them for their relevance to the rapid excavation process in hard rock.

2.0 DYNAMICS AND FRACTURE OF ROCK

Dynamic behavior of rock is significant from the point of view of rapid excavation. Methods of rapid excavation in hard rock must use some form of dynamic or impact loading by means of explosives, water jet, etc. The phenomena of interest under these conditions are stress waves, dynamic stresses and deformations and fracture initiation and propagation.

The problem of wave propagation in isotropic elastic media has been dealt with extensively by analytical and experimental methods. As described by Kolsky[2] in his monograph on stress waves, a dynamic loading in an infinite medium generates two types of waves, a dilatational wave propagating with a velocity of

$$c_1 = \sqrt{\frac{\lambda + 2\mu}{\rho}} \tag{1}$$

and a distortional wave propagating with a velocity of

$$c_2 = \sqrt{\frac{\mu}{\rho}} \tag{2}$$

where

c_1, c_2 = dilatational and distortional wave propagation velocities

λ, μ = Lame' constants

ρ = density

In addition to these two basic types of waves a third type occurs along free surfaces. This wave, referred to as Rayleigh wave, travels with a velocity slightly lower than that of the distortional wave. The intensity of these waves decreases rapidly with depth below the surface.

Wave propagation in a medium is defined by the loading characteristics (time and space variation of loading), geometry of the body and material properties. Wave propagation in rock media is a more complex phenomenon due to the intrinsic properties of rock, such as anisotropy, inhomogeneity and presence of discontinuities and flaws. Thus, propagation velocities may be different in different directions. Wave propagation may also be frequency dependent due to both inelasticity of the material and to inhomogeneity. The latter becomes significant for steep loading pulses when wavelengths become of the same order of magnitude as the grains and discontinuities.

Little work has been reported on wave propagation in rock media. Bienawski[3] has measured dilatational, distortional and Rayleigh wave velocities in norite, where it appears that these velocities do not have the same relative magnitudes that would be predicted theoretically. This points to the need for knowing the dynamic properties of the material. Ricketts and Goldsmith[4] have measured dynamic properties in rock using a Hopkinson bar system.

The problem of fracture and crack propagation in rock is even more complex than that of wave propagation. Griffith's theory of brittle fracture states that crack propagation occurs when very high tensile stresses are induced at the tips of pre-existing cracks or flaws in the material.[5] This theory was further modified by McClintock and Walsh[6] to account for the closing of cracks in a compressive stress field, and verified experimentally by Hoek[7] who used it to explain failure around openings in rock.

According to the Griffith criterion fracture initiation takes place when

$$\sigma = \sigma_{in.} = \sqrt{2\gamma E/\pi c_o} \qquad (3)$$

where

σ = applied uniaxial tensile stress

$\sigma_{in.}$ = value of σ when crack propagation starts

γ = specific surface energy

E = Young's modulus

c_o = half-length of preexisting crack

An alternate form of this criterion given by Irwin[8] and applied by Bienawski[3] to rock is

$$\sigma = \sqrt{GE/\pi c} \tag{4}$$

where G is the energy released per unit crack surface area. Fracture propagation is stable as long as there is a definite relationship between σ and c. When this relationship ceases to exist and crack growth Δc is not controlled by the stress increment $\Delta\sigma$, crack growth becomes unstable. This happens when the energy release rate reaches a critical value G_c. Then,

$$\sigma = \sigma_u = \sqrt{G_c E/\pi c_u} \tag{5}$$

where σ_u = value of stress when fracture propagation becomes unstable

c_u = corresponding crack half-length

The critical value G_c is a characteristic property of the material.

When crack growth becomes unstable, crack propagation velocity becomes important. Crack propagation is a dynamic phenomenon and has been treated as such by Yoffe,[9] Roberts and Wells[10] and Baker.[11] In these analyses, the problem is treated either as one of dynamic elasticity or, in the case of the energy approach, account is taken of the kinetic energy of the material particles around the propagating crack. One result

of these analyses, subsequently verified by Wells and Post,[12] is that dynamic stress distributions are not appreciably different from static ones. Another significant conclusion is that the crack velocity reaches a terminal value

$$v_t = \sqrt{2\pi/k}\sqrt{E/\rho} \tag{6}$$

or, for $\nu = 0.25$,

$$v_t = 0.38\sqrt{E/\rho} \tag{7}$$

or

$$v_t = 0.5\sqrt{\frac{\mu}{\rho}} \tag{8}$$

Once the terminal fracture velocity is reached crack branching or bifurcation occurs, so that increasing energy is released through additional crack surfaces. The attainment of this terminal velocity coincides with ultimate failure of the material.

Experimental investigations on crack propagation in glass have been pioneered by Schardin[13] who introduced the multiple-spark camera (Schardin camera). Wells and Post[12] used dynamic photoelasticity with transparent plastic models. Fracture propagation in rock has been studied by Hoek and Bienawski[3,14-16] using high-speed photography.

In addition to fundamental fracture mechanics of rock the whole phenomenon of rock blasting has been studied in the laboratory. Persson[17] used high-speed photography and plexiglas and glass models because of their rock-like fracture behavior. In a series of scale model blastings, various fracture phenomena associated with cylindrical boreholes were observed and correlated with derived stresses in the material. The boreholes were charged with PETN-powder to different densities, thereby realizing a variety of detonating pressures. The predicted

fracture mechanisms initiated by the gas pressure and influenced by the reflecting shock waves were verified. Both two- and three-dimensional studies were conducted.

The interaction of reflected shock waves and radial cracks moving out from a single borehole has been investigated by Field and Ladegaard-Pedersen.[18] A tensile wave passing the material in front of a crack tip will contribute to the stress field with a tensile stress component normal to the fracture plane and the fracture velocity will increase. According to Field those cracks travelling in directions forming an angle of 40-80 degrees to the normal on the free surface are accelerated.

3.0 EXPERIMENTAL METHODS

3.1 Dynamic Photoelasticity

In dynamic photoelasticity, as in the static case, a model is fabricated out of a birefringent material and subjected to dynamic loadings similar to those encountered in the prototype. The model is viewed in monochromatic polarized light and the resulting isochromatic fringe patterns are recorded by means of appropriate electronic and photographic instrumentation.

The interpretation of fringe orders is the same as in the static case, i.e., the fringe order is related to the principal stress difference by the stress-optic law

$$\sigma_1 - \sigma_2 = \frac{2nf_\sigma}{h} \tag{9}$$

where

f_σ is the material fringe value

h is the model thickness.

The value of f_σ is determined by suitable calibration for a dynamic loading of similar duration and rate as the one used in the model.

The separation of stresses, i.e., the determination of individual values of σ_1 and σ_2, requires additional experimental data, such as strains. The moiré method of strain analysis has been used extensively for this purpose. In certain specific cases of wave propagation, however, principal stress separation is possible without any additional data. In the case of a pure dilatational wave, principal stresses act in the direction of wave propagation and perpendicular thereto; however, deformations occur only in the direction of wave propagation. Thus, the displacements are:

$$u_r = f(r),\ u_\theta = 0 \tag{10}$$

For a point source, the incident P_1 wave exhibits polar symmetry, which makes possible the determination of individual strains (and stresses) from purely photoelastic data as follows:

$$\varepsilon_\theta = \frac{u_r}{r} = -\frac{(1+\nu)}{E}\,\frac{f_\sigma}{h}\int_r \frac{n}{r}\,dr \tag{11}$$

$$\varepsilon_r = \varepsilon_\theta - \frac{1+\nu}{E}\,\frac{n}{h}\,f_\sigma \tag{12}$$

Separation of principal stresses using only photoelastic data is also possible in the case of a pure distortional wave (S type) since for a state of pure shear it is known that

$$\sigma_1 = -\sigma_2 \tag{13}$$

Thus, it is seen that separation of principal stresses is easily accomplished whenever there is a distinct separation of P and S waves.

Most birefringent materials used in model studies are viscoelastic in nature and, therefore, exhibit rate (or time, or frequency) dependence in all mechanical and optical properties. Whenever material behavior is such that rate effects cannot be neglected, a photoviscoelastic analysis of the fringe patterns is necessary. Methods and techniques for such an analysis have been developed and successfully applied to wave propagation problems. The stress-optic law in this case takes more complicated forms, involving a time-dependent stress fringe value which must be determined by proper dynamic calibration tests.

3.2 Birefringent Coating Method

While the conventional method of transmission photoelasticity is not feasible with opaque rock materials, the birefringent coating technique is ideally suited for determining the surface strains in such materials. Knowledge of the strain field and the stress-strain response for the rock enables evaluation of the stress field. Numerous studies have also been

conducted to further develop the method and to establish the accuracy of the technique under various practical conditions.

The birefringent coating technique consists of bonding a thin sheet of photoelastic material to the structure, in this case the rock. When the rock structure is loaded, the surface deformations and strains of the rock are transferred to the bonded coating and induce a birefringence in the latter. The birefringence is observed and recorded by means of a reflection polariscope, where the polarized light traverses the thickness of the coating and is reflected back from a reflective layer provided at the interface between the coating and the structure. Within the linear strain-optic range of the coating, the fringe patterns are directly related to the surface deformations (and strains) in the structure whether they are elastic or not. While strain gages provide point-by-point results, photoelastic coatings give full-field information. Moreover, coatings provide instantaneous visual observation of the strain field throughout the loading pulse.

At any generic point, the relative retardation fringe order n of the photoelastic coating is related to the difference in the in-plane principal strains in the rock ε_1, ε_2 by the strain-optic law:

$$\varepsilon_1 - \varepsilon_2 = \frac{n\lambda}{2tK} = \frac{nf_\varepsilon}{2t} \tag{14}$$

where

t = coating thickness

λ = wavelength of light

K = strain sensitivity coefficient

f_ε = strain fringe value of coating material

In those cases where the material response is linearly elastic, the observed birefringence in the coating is related to the principal stresses σ_1, σ_2 in the structure (rock) by

$$\sigma_1 - \sigma_2 = \frac{nf_\varepsilon}{2t} \frac{E}{(1 + \nu)} \tag{15}$$

where E and ν are the elastic modulus and Poisson's ratio of the material.

The accuracy of the coating technique is influenced by the mismatch in Poisson's ratio between the rock and coating. While the Poisson's ratio for the rock materials is lower than that of the coating, the mismatch effect can be minimized by using thin coatings. However, thin coatings produce fewer fringes as can be seen from Eq. (14). The mismatch in Poisson's ratio becomes significant over a transition zone between a free boundary of a specimen and the internal region. Photoelastic coatings are ideal for detecting visually regions of plastic deformation, fracture initiation and propagation. Photoelastic coatings have been applied successfully to the study of strain distribution and fracture around cavities in rock.[19,20]

3.3 Moiré Method

The moiré effect is an optical phenomenon observed when two closely spaced arrays of lines are superimposed and viewed with either transmitted or reflected light. If the two arrays consist of opaque parallel lines which are not identical in either spacing (pitch) or orientation, then interference between the two arrays occurs and moiré fringes are produced. The concept offers a reasonably easy means of full-field in-plane displacement and strain analysis. Being strictly geometric in nature, the technique is independent of the anisotropy and the stress-strain response of the material. The in-place displacement field is measured directly and the strain fields are derived by differentiation of these displacement fields.

In actual practice, one array is photo-printed, etched, or bonded on the surface of the specimen. A transparent reference array usually of the same pitch is placed adjacent to the specimen and aligned parallel to the specimen array. As the specimen is loaded, the specimen array will deform and follow the surface displacements induced by the loads. The reference array, of course, does not deform since it is not loaded and as a consequence a moiré interference pattern forms when light is transmitted through the two arrays.

Moiré fringe patterns can most easily be interpreted by relating them to the displacement field since moiré fringes are loci of points having the same component of displacement in a direction perpendicular to the grid lines of the undistorted reference array. Once two orthogonal displacement fields (u and v) have been established by using line arrays parallel to the x and y axes of a specimen, the cartesian strain components can be computed from the derivatives of the displacements. For small strains these relations take the form:

$$\varepsilon_x = \frac{\partial u}{\partial x}$$

$$\varepsilon_y = \frac{\partial v}{\partial y} \qquad (16)$$

$$\gamma_{xy} = \frac{\partial u}{\partial y} + \frac{\partial v}{\partial x}$$

where

x,y = cartesian reference axes

u,v = x and y components of the displacement

$\varepsilon_x, \varepsilon_y$ = normal components of strain

γ_{xy} = shear component of strain

The displacement gradients $\partial u/\partial x$ and $\partial v/\partial y$ are obtained from the slopes of the two displacement surfaces in a direction perpendicular to the lines of the reference arrays. The displacement gradients $\partial u/\partial y$ and $\partial v/\partial x$ are obtained from the slopes of the displacement surfaces in a direction parallel to the lines of the reference array.

The fineness of the line images required to obtain satisfactory information from a moiré pattern depends only upon the magnitude of the deformations. However, these deformations are in turn related to the modulus of elasticity of the specimen material, the geometry of the specimen, and the manner of loading. Line spacings for a given material can only be specified over a broad range. The pitch of the array should be small enough to give sufficient response even in cases where the material is stressed below the yield point (in the case of elastic analyses). On the other hand, the pitch should not be so fine as to produce fringes that can no longer be clearly distinguished. The moiré method is well suited for the study of transient displacement (hence strain) fields and fracture propagation in dynamically loaded rock specimens.

4.0 WAVE AND CRACK PROPAGATION IN ROCK-LIKE MEDIA

4.1 Experimental Procedure

The materials used in this phase of the program were transparent birefringent materials to allow the application of dynamic photoelastic techniques. Three different materials were used, Columbia Resin (CR-39), Polyester Resin (Homalite 100), and Plexiglas. The specimens were 10 in. x 6 in. plates 1/4 in. and 1/8 in. thick. Thirteen specimens were tested by means of explosive loading. Most specimens were loaded through an internal 1/2 in. diameter hole located along the long centerline 2.5 in. from one end (Fig. 1a). A 1/2 in. long radial slot was sawed at one point on the hole boundary along the horizontal centerline to facilitate crack initiation at that point. Some specimens were loaded through a slot at one end (Fig. 1b).

Explosive loading was produced by detonating 50 mg and 100 mg charges of Pentaerythritol Tetranitrate (PETN). This explosive is readily available in Primacord and is well suited for dynamic loading of models. Typical pulses produced by PETN have a rise time of approximately one microsecond and a mean width of six microseconds. Furthermore, PETN explosions do not produce too much smoke or light, thus allowing photography of fringe patterns near the explosive source.

The PETN powder was dissolved in acetone and precipitated in ice water to obtain a finer particle size. This powder was then pressed into specially made plexiglas detonator caps. The cap with the explosive was attached to an exploding bridge wire header. The EBW header consisted of two terminal pins embedded in a plastic cylinder. The terminal pin spacing is bridged with 0.0015 in. diameter gold wire. When a high voltage (2000v) is rapidly (in 1 μ sec) imposed across the header terminals the gold wire explodes and initiates the detonation of the fine grain PETN in contact.

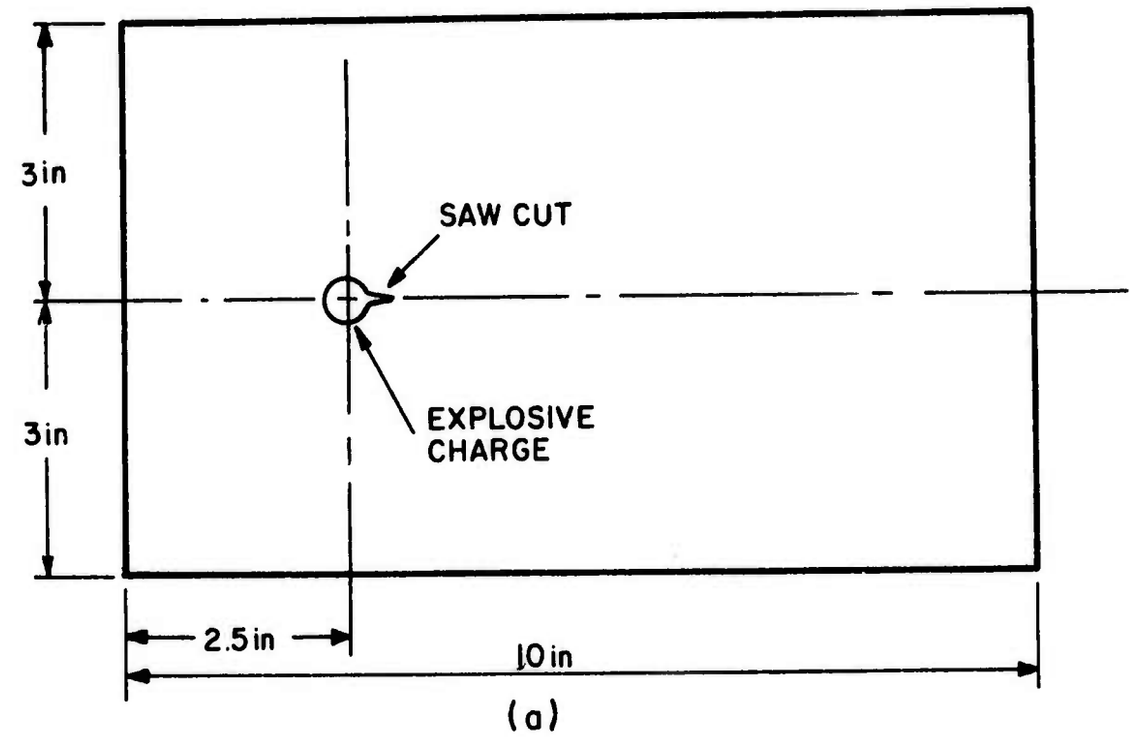

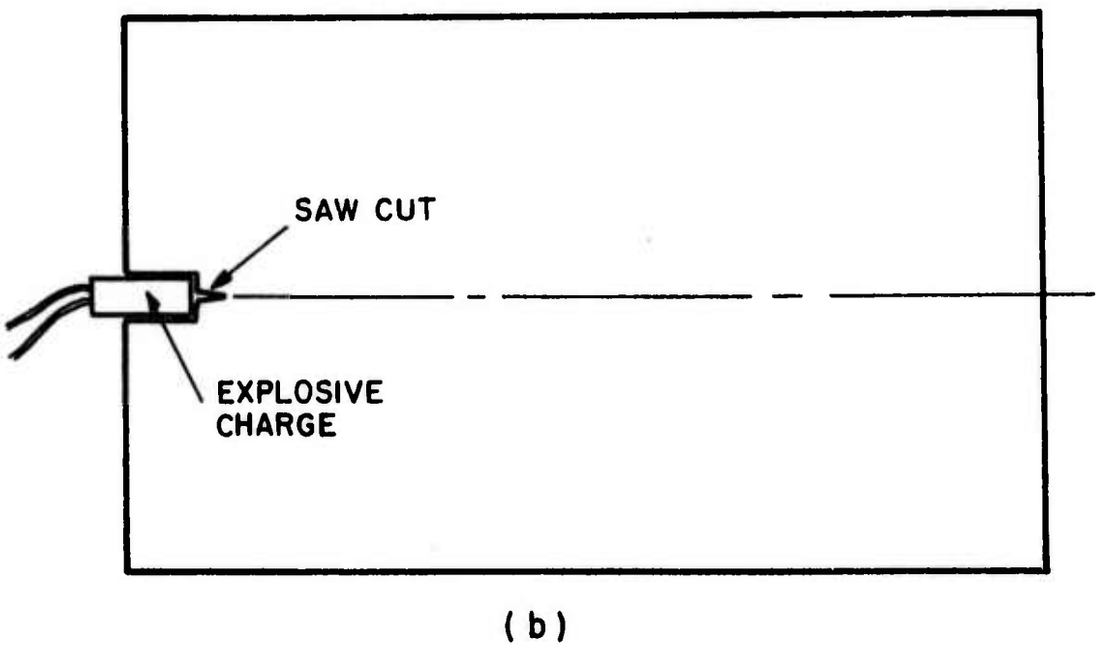

Fig. 1 DIMENSIONS AND LOADING OF TRANSPARENT PHOTOELASTIC SPECIMENS. (a) INTERNAL LOADING (b) END LOADING

Dynamic photoelastic fringe patterns were recorded by a multiple spark camera (Cranz-Schardin). This camera system is capable of photographically recording a time-sequenced series of 16 dynamic photoelastic fringe patterns at rates that can be varied between 185,000 and 700,000 frames per second. The line definition of the photographic records is such that an array of approximately 12 lines per inch moving at a velocity of 100,000 in./sec can be resolved.

The light source is provided by a 4 by 4 array of 16 separate spark gaps discharged sequentially. The exact time and sequence of firing is sensed with a photosensitive device (Lite mike) and recorded with an oscilloscope. The light from each spark gap passes through a circular polaroid element, the model and a second circular polaroid element. It is then collected by a 9-in. diameter field lens and is focused on one of 16 camera lenses. To obtain a narrow bandwidth of light, gelatin filters (No. 47B) having a maximum transmission between 4,200 and 4,400 angstroms were placed behind the camera lenses. The 16 images obtained are recorded on a large (11 in. x 14 in.) sheet of Kodak Commercial Film No. 4127.

In operation of the system, a number of events were coordinated; the detonation of the explosive charge, the triggering of the oscilloscope and the triggering of the spark gap bank. The sequence of events was initiated by means of a firing circuit emitting simultaneously three pulses: (1) a 2 kv pulse which exploded the bridge wire and detonated the PETN, (2) a 20 v pulse which triggered the oscilloscope, and (3) a 20 v pulse which triggered the spark gap bank through a time delay generator.

Four 1/4 in. thick CR-39 specimens were loaded with 100 mg PETN charges, and two 1/8 in. thick CR-39 specimens were loaded with 50 mg charges. Two 1/4 in. thick Plexiglas plates were loaded with 100 mg charges and two 1/8 in. thick

Homalite-100 plates were loaded with 50 mg charges. The resulting fringe and crack patterns were recorded by the Cranz-Schardin camera at a rate of 180,000 frames per second.

4.2 Results and Discussion

Typical records of dynamic fringe patterns in 1/8 in. and 1/4 in. thick CR-39 specimens loaded with 50 mg and 100 mg charges of PETN are shown in Figs. 2 and 3. The propagation velocities of various fringe orders were computed from such records and plotted versus fringe order in Fig. 4. The results show some spread due to the variation of specimen thickness and amount of explosive charge. The wavefront velocity obtained by extrapolation to the zero fringe order varied between 75,500 in./sec and 80,000 in./sec. The velocity of the shear waves reflected from the free edges of the specimen was also measured. It varied between 38,700 in./sec and 41,500 in./sec, the higher value obtained from the 1/8 in. thick specimen (No. 7). This velocity can also be calculated from the measured dilatational plate velocity and Poisson's ratio as follows:

$$c_s = c_L \sqrt{\frac{1-\nu}{2}} \qquad (17)$$

where c_s = shear velocity

c_L = dilatational plate velocity

ν = Poisson's ratio

For an average value of c_L = 78,000 in./sec and ν = 0.35, c_s = 44,400 in./sec.

Excessive crack branching was observed in all specimens due to the high energy of the explosive charge. Final crack patterns for CR-39 specimens No. 4, 6, and 7 are shown in Fig. 5. The crack propagation velocities varied more widely than wave propagation velocities. They were 17,200, 14,000, 20,000 and 20,500 in./sec for specimens No. 4, 6, 7, and 13.

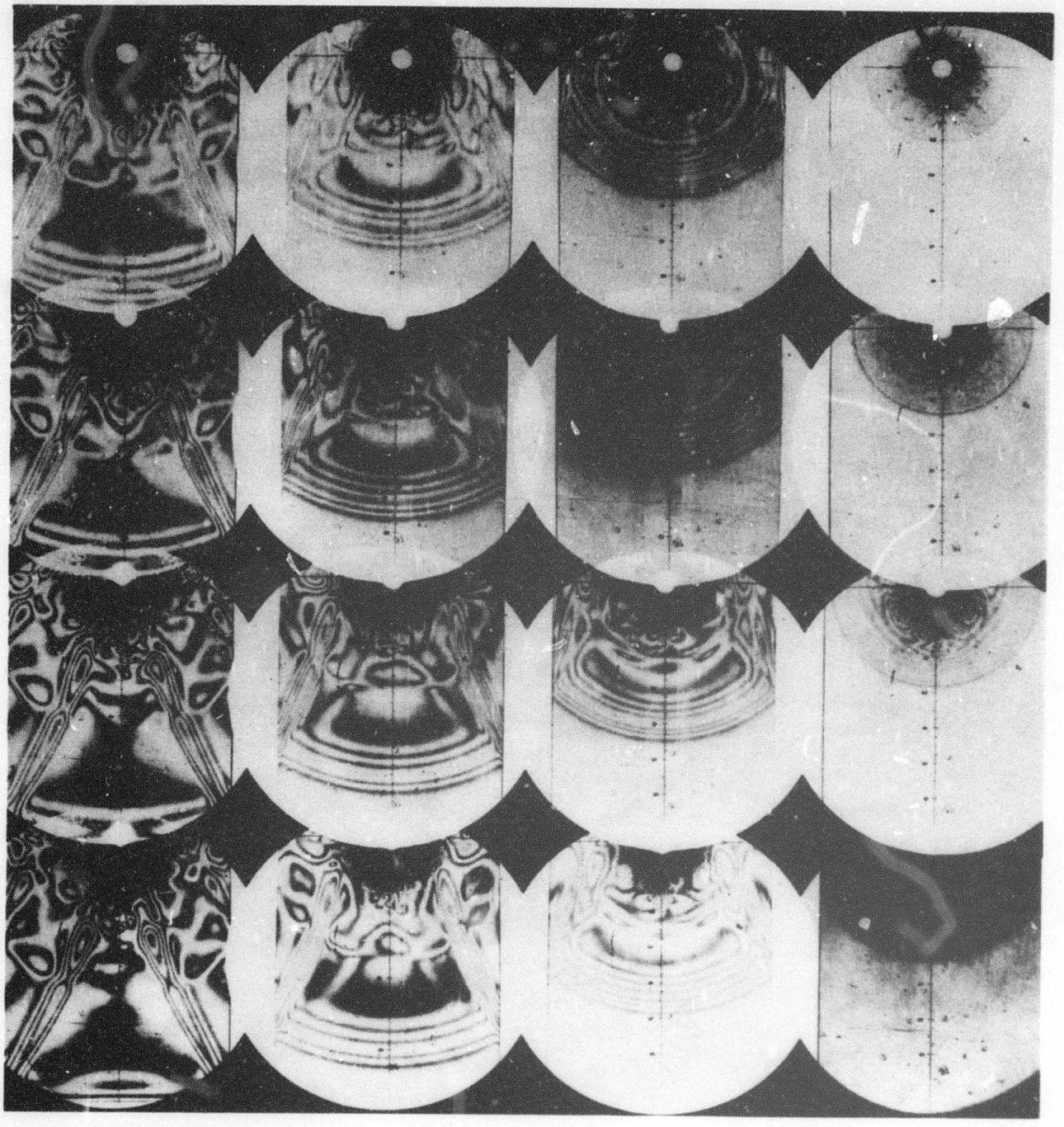

Fig. 2 ISOCHROMATIC FRINGE PATTERNS IN SPECIMEN NO. 7 (1/8 IN. THICK CR-39; 50mg PETN CHARGE; CAMERA SPEED 175,000 FRAMES PER SECOND)

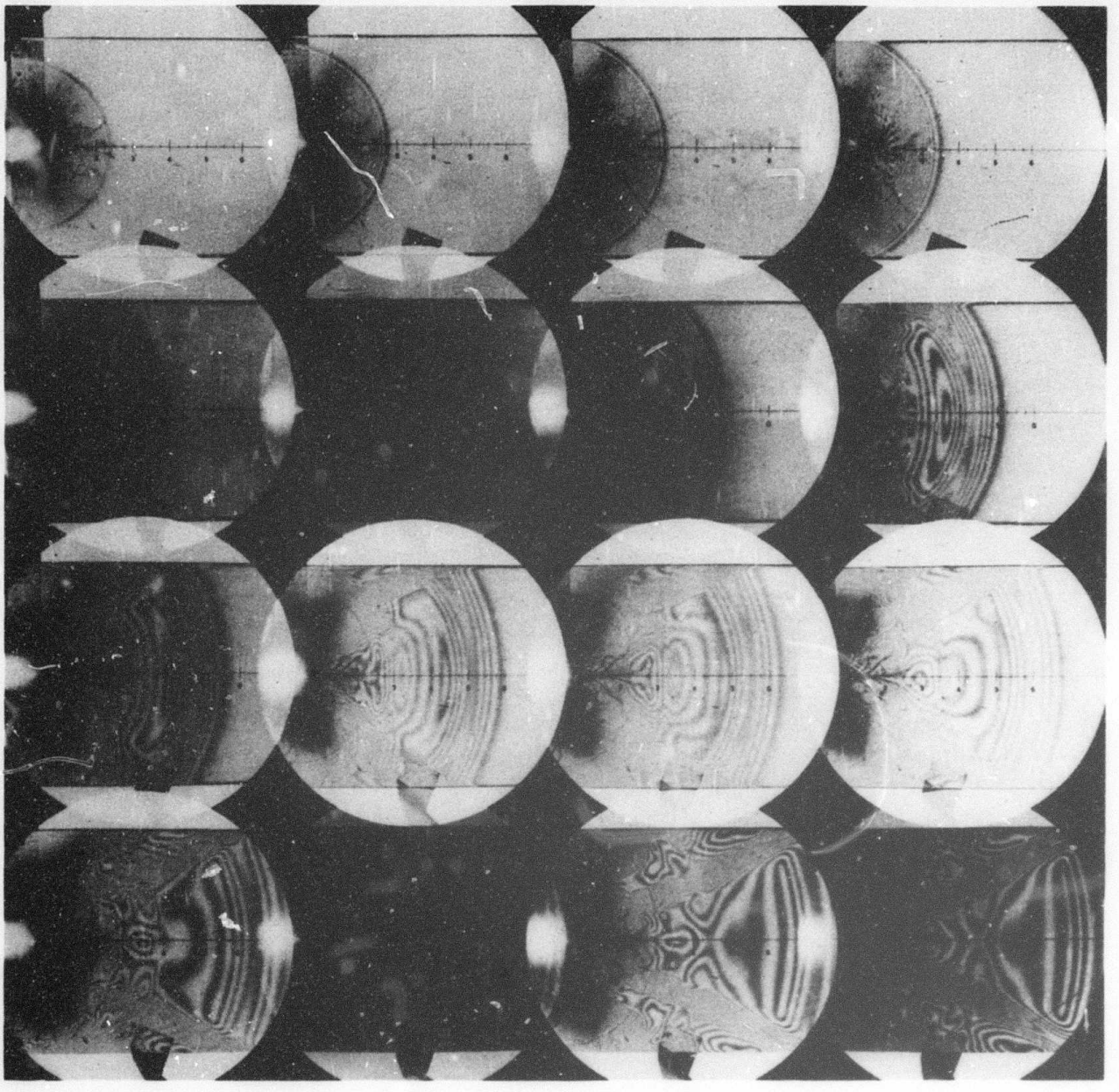

Fig. 3 ISOCHROMATIC FRINGE PATTERNS IN SPECIMEN NO. 13 (1/4 in. Thick CR-39; 100 mg PETN Charge; Camera Speed 180,000 Frames Per Second)

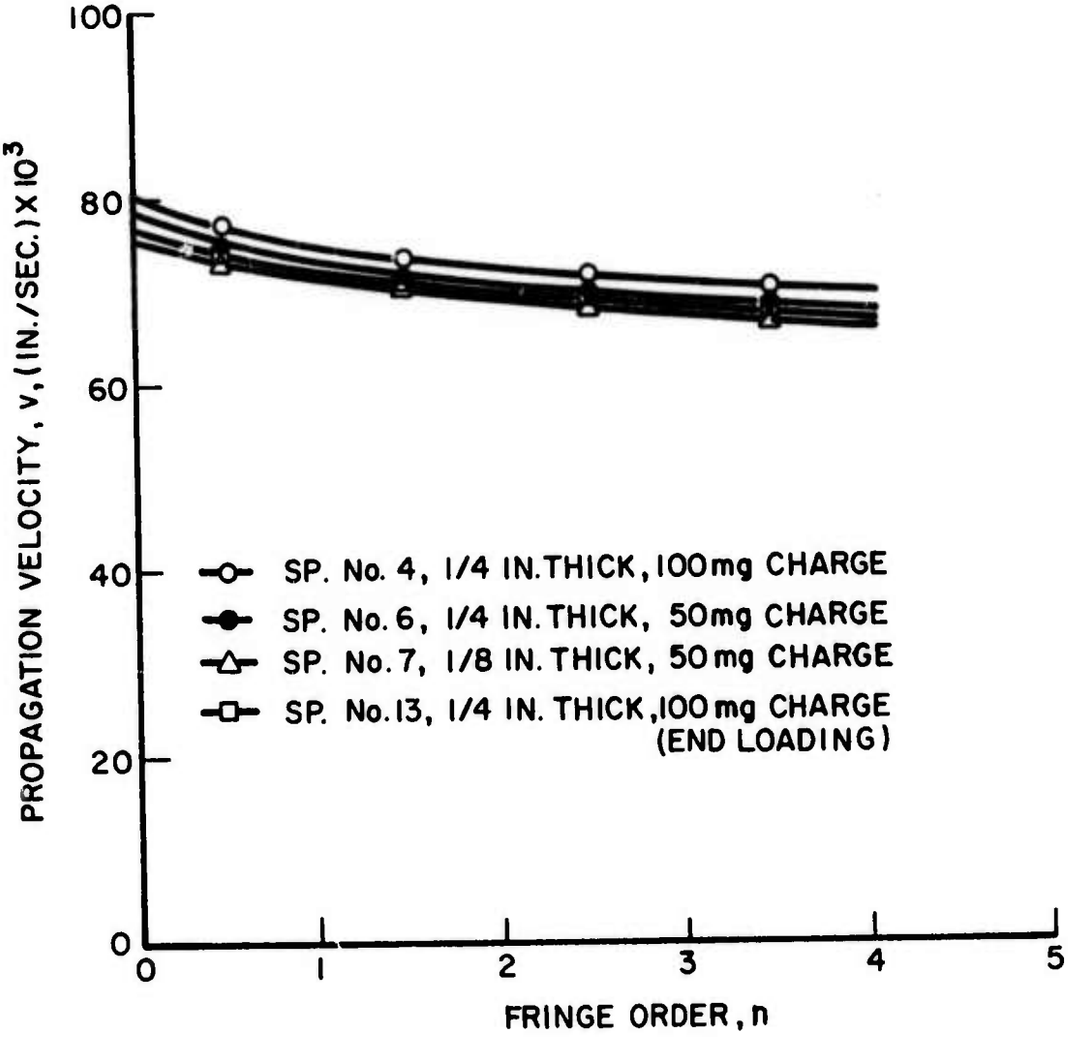

Fig. 4 WAVE PROPAGATION VELOCITY AS A FUNCTION OF FRINGE ORDER IN CR-39 SPECIMENS

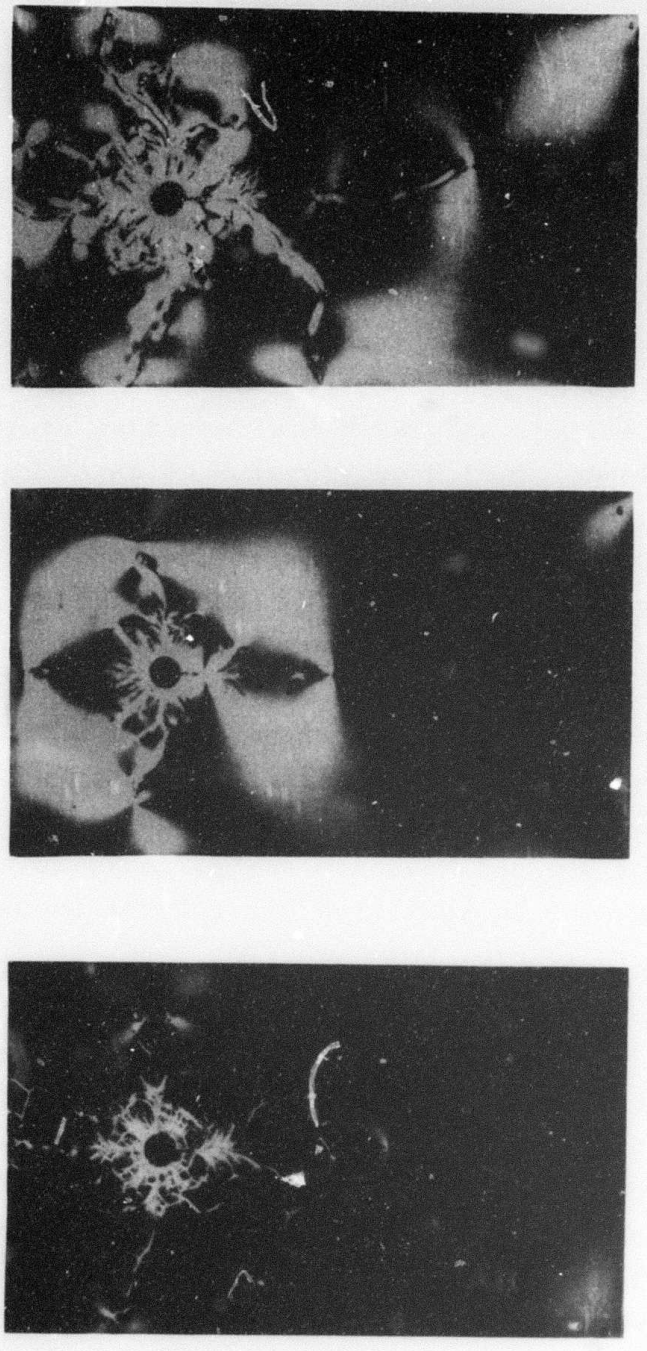

Fig. 5 FINAL CRACK PATTERNS IN CR-39 SPECIMENS NO. 4 (1/4 in. THICK, 100 mg CHARGE), NO. 6 (1/4 in. THICK, 50 mg CHARGE), AND NO. 7 (1/8 in. THICK, 50 mg CHARGE)

Wave and crack propagation results for CR-39 obtained from four tests are summarized in Table 1. It is seen that the maximum ratio of the crack propagation velocity to the shear wave velocity is 0.50, equal to the theoretical prediction.[21] The lowest ratio was found for the 1/4 in. thick specimen with the 50 mg explosive charge.

Tests similar to those described above were conducted with Plexiglas and Homalite-100 specimens. A typical record of dynamic fringe patterns in a Plexiglas specimen is shown in Fig. 6. The propagation velocity as a function of fringe order is plotted in Fig. 7. The wavefront velocity, obtained by extrapolation to the zero fringe order, is 96,000 in./sec. The shear wave velocity was obtained by three different ways. The velocity of the incident shear wave visible in the fringe patterns of Fig. 6 is 53,700 in./sec, that of the shear wave reflected from the free edges is 50,000 in./sec, and that calculated from the measured dilatational wave with an assumed value of 0.35 for Poisson's ratio is 54,600 in./sec. A very limited amount of cracking was observed because of the more pronounced viscoelasticity and ductility of the material.

Dynamic fringe patterns in 1/8 in. thick Homalite-100 plates loaded with 50 mg PETN charges are shown in Figs. 8 and 9. Figure 8 shows the first stage of the phenomenon covering the period between 23 μsec and 130 μsec after loading, and Fig. 9 covers a later stage between 87 μsec and 175 μsec after loading. The propagation velocity as a function of fringe order is plotted in Fig. 10. The wave-front velocity obtained by extrapolation is c_L = 89,000 in./sec. The incident shear wave velocity is 49,500 in./sec, and the one computed from the measured dilatational velocity is 50,500 in./sec. Cracking again was limited and the maximum crack propagation velocity observed was 13,500 in./sec, far below the limiting theoretical value of 25,000 in./sec. Final crack patterns of the two Homalite-100 specimens are shown in Fig. 11. The pattern of

Table 1

WAVE AND CRACK PROPAGATION IN CR-39

Specimen Thickness, in.	Explosive Charge, mg	Type of Loading	Dilatational Plate Velocity, c_L, in./sec	Measured Shear Wave Velocity, c_s, in./sec	Crack Propagation Velocity, v_{cr}, in./sec	Velocity Ratio v_{cr}/c_s
1/4	100	Internal	80,000	38,700	17,200	0.45
1/4	50	Internal	78,500	39,600	14,000	0.35
1/8	50	Internal	75,500	41,500	20,000	0.48
1/4	100	End	77,000	41,400	20,500	0.50

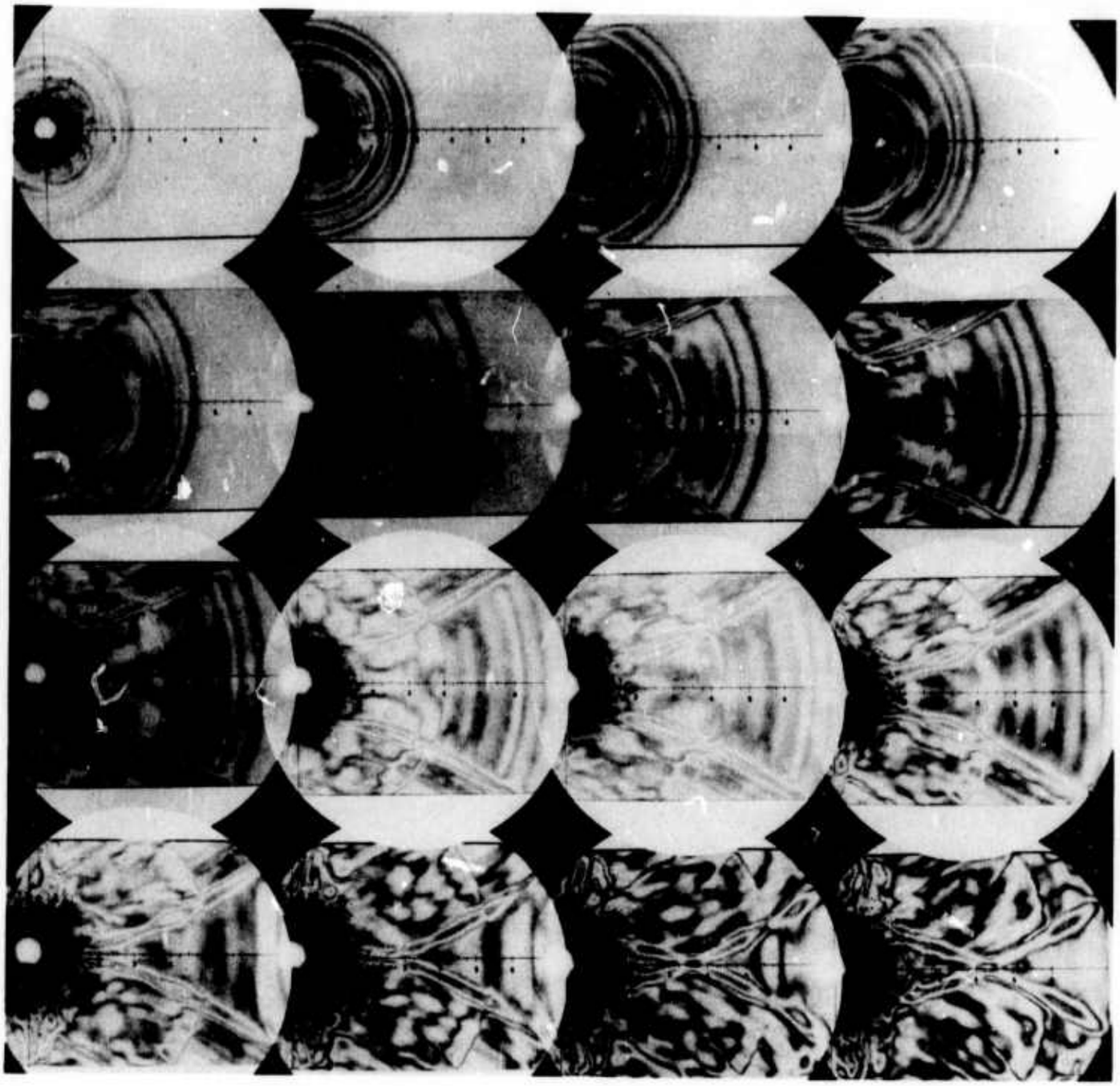

Fig. 6 ISOCHROMATIC FRINGE PATTERNS IN SPECIMEN NO. 8 (1/4 in. Thick Plexiglas; 100 mg PETN Charge; Camera Speed 180,000 in./sec)

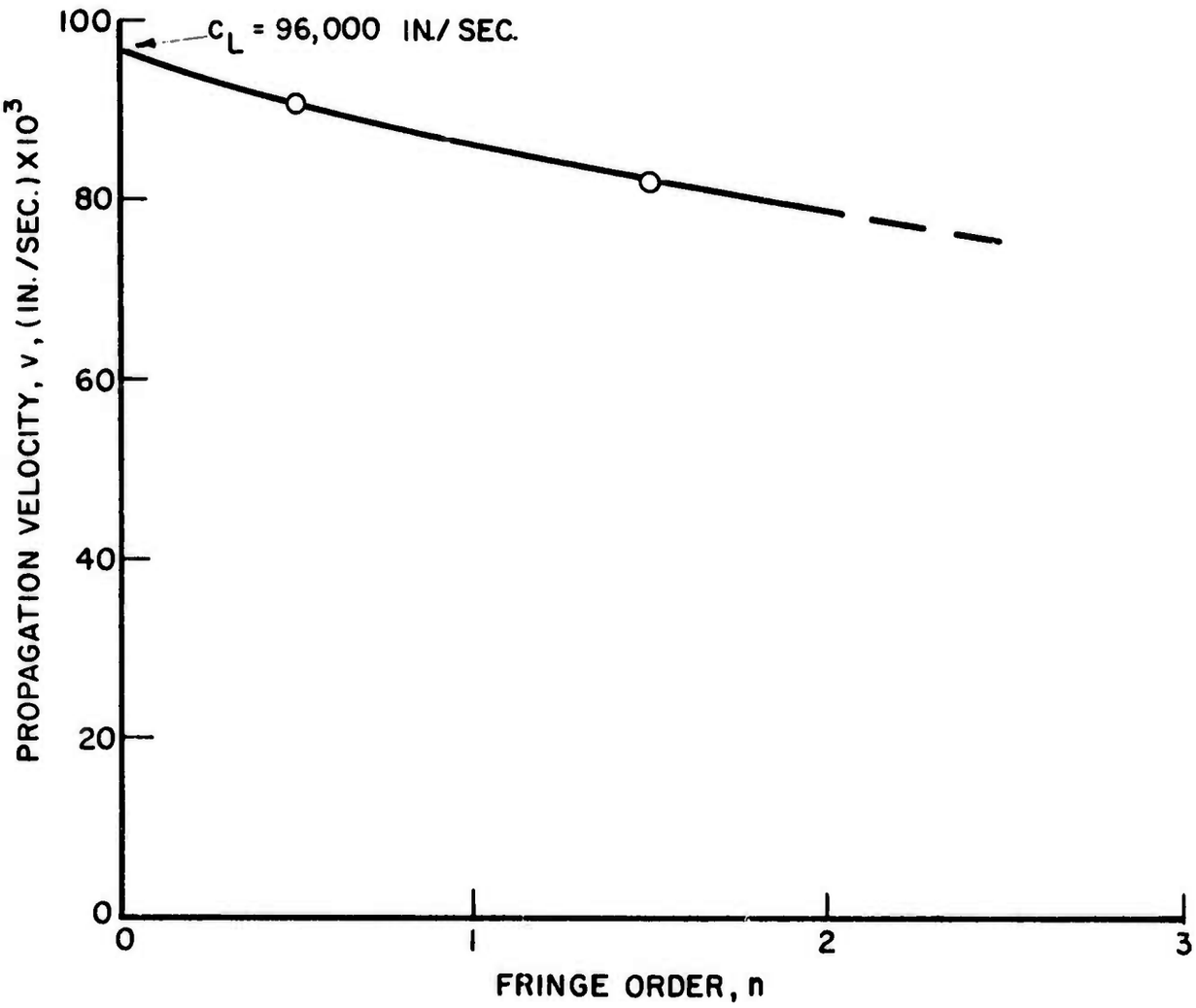

Fig. 7 WAVE PROPAGATION VELOCITY AS A FUNCTION OF FRINGE ORDER IN PLEXIGLAS SPECIMEN

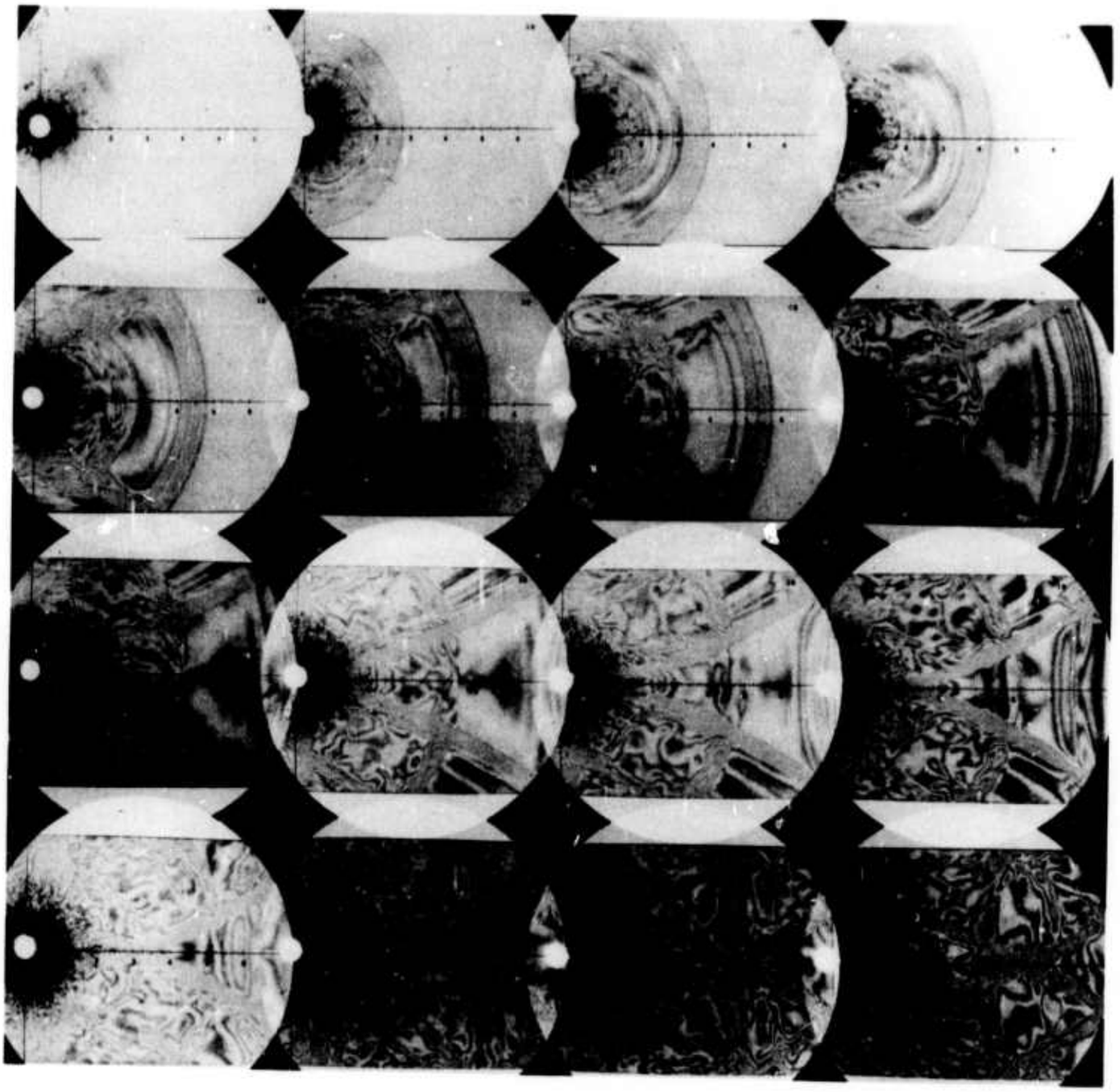

Fig. 8 ISOCHROMATIC FRINGE PATTERNS IN SPECIMEN NO. 10 (1/8 in. Thick Homalite-100; 50 mg PETN Charge; Average Camera Speed 146,000 Frames Per Second; Time Interval 23 μsec to 130 μsec After Loading)

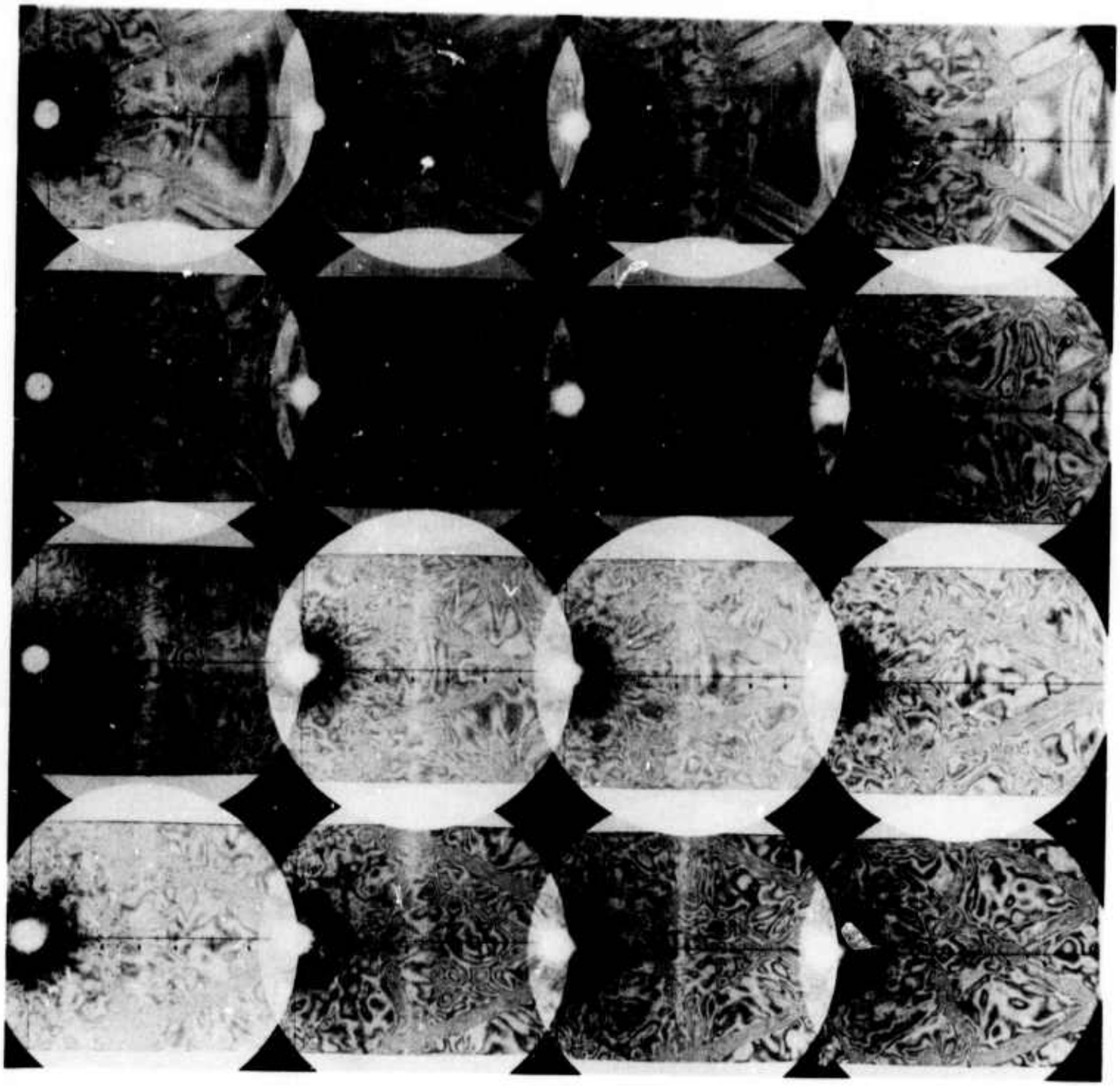

Fig. 9 ISOCHROMATIC FRINGE PATTERNS IN SPECIMEN NO. 11 (1/8 in. Thick Homalite-100; 50 mg PETN Charge; Average Camera Speed 170,000 Frames Per Second; Time Interval 87 μsec to 175 μsec After Loading)

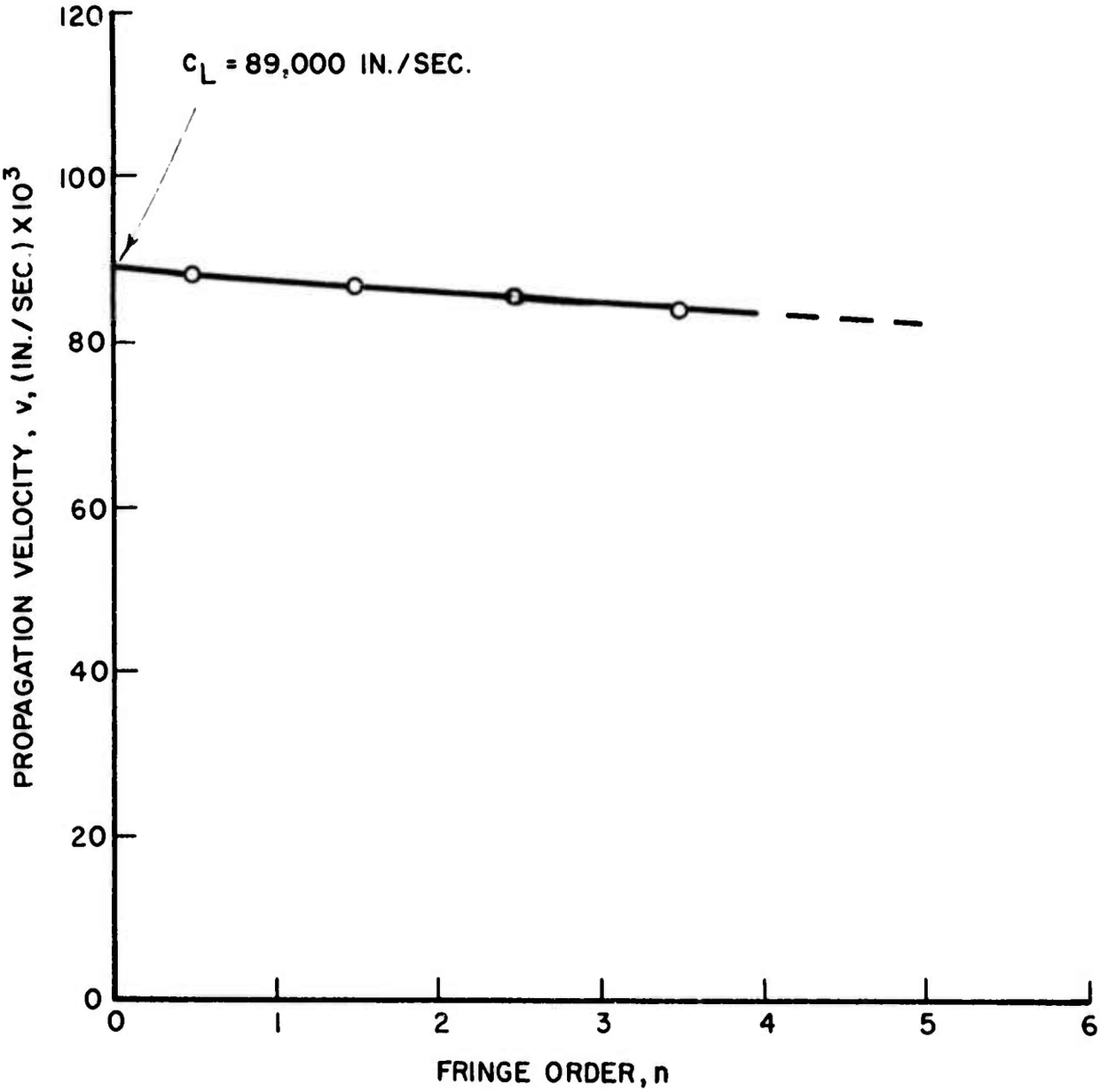

Fig. 10 WAVE PROPAGATION VELOCITY AS A FUNCTION OF FRINGE ORDER IN HOMALITE-100 SPECIMEN

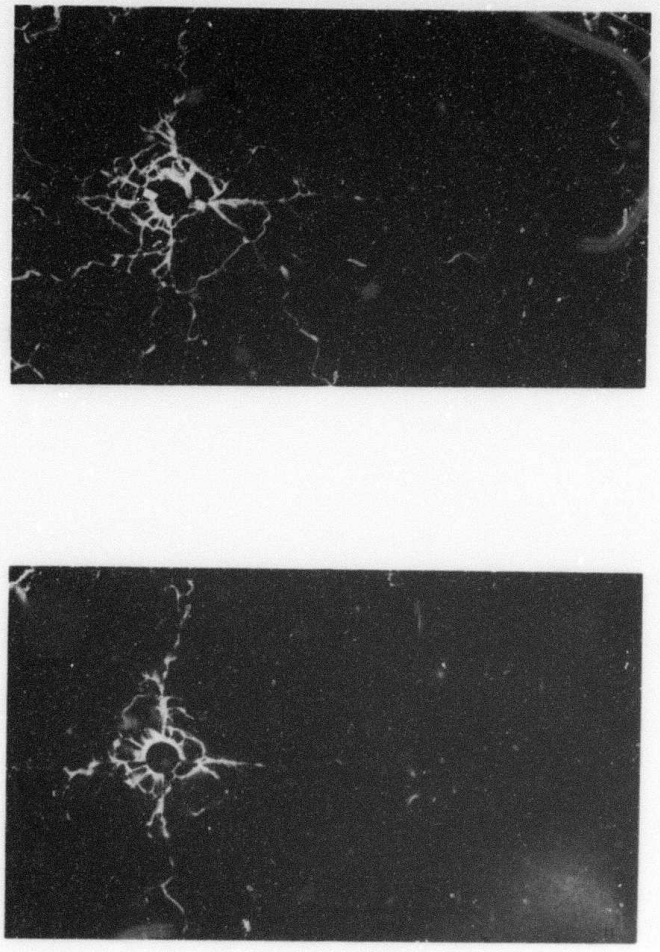

Fig. 11 FINAL CRACK PATTERNS IN HOMALITE-100 SPECIMENS NO. 10 AND 11

specimen No. 10 shows excessive crack branching with both radial and circumferential cracking around the loaded hole. Spalling at the corners and at the edge farthest from the hole due to reflected tensile waves is plainly visible.

5.0 WAVE PROPAGATION IN ROCK MEDIA

5.1 Uniaxial Wave Propagation

Vermont marble and Cold Spring (Minnesota) granite were the two rock media investigated.* Bar specimens of dimensions 1/2 in. x 1/2 in. x 12 in. were used to determine uniaxial wave propagation and the dynamic tensile strength of these materials.

The stress-wave technique has been employed for this purpose to determine the dynamic properties of brittle materials.[22] A slender, freely supported bar is impulsively loaded at one end and strains or displacements are measured at one or two stations along the bar. The wave propagation velocity is determined from the travel time of the pulse between two stations. This uniaxial wave velocity is related to the dynamic modulus of the material (E) and its density (ρ) by

$$c_o = \sqrt{\frac{E}{\rho}} \tag{18}$$

The stress at any point can be determined from measurement of either the axial strain or the particle velocity at that point. The axial stress is determined by the following relationships:

$$\sigma_x = \rho c_o \frac{\partial u}{\partial t} = E\varepsilon_x \tag{19}$$

where

σ_x = axial stress

$\frac{\partial u}{\partial t}$ = particle velocity at point in question

ε_x = axial strain at point in question

*The granite was supplied free of charge by the Cold Spring Granite Company, Cold Spring, Minnesota.

The equations above are based on the assumptions that (1) the material is linear elastic, (2) lateral inertia forces are negligible, and (3) all cross sections of the bar remain plane during deformation.

Tensile strength measurements using the wave propagation technique depend on the phenomenon of stress-wave reflection from a free boundary. The compressive pulse introduced at one end of the bar is reflected as a mirror-image tensile pulse. Since the tensile strength of rocks is much lower than the compressive strength, the bar fails in tension upon reflection of the pulse from the free end.

Marble and granite bars were instrumented with strain gages at two stations located 4 in. from each end (Fig. 12). The gages were connected to potentiometric circuits and their signals recorded on an oscilloscope. Preliminary tests were conducted by dropping a steel ball on the end of the bar from heights of 19 in. and 38 in. Typical records obtained from marble specimens are shown in Fig. 13. These signals show appreciable attenuation and wave scattering due to internal friction losses in the material. Propagation velocities computed from these records are relatively low, the highest velocity measured being 100,000 in./sec. Similar tests on granite bars gave wave velocity values of the order of 160,000 in./sec, which are lower than expected.

The specimens were subsequently loaded at one end with explosive charges (R. Stresau Laboratories, N-1 detonators, approximately 50 mg total charge). Figure 14 shows strain gage data from one of these tests in marble. Appreciable scatter was noticed in the measured wave propagation velocities. The average of five measurements gave a value of

$$c_o = 155{,}000 \text{ in./sec}$$

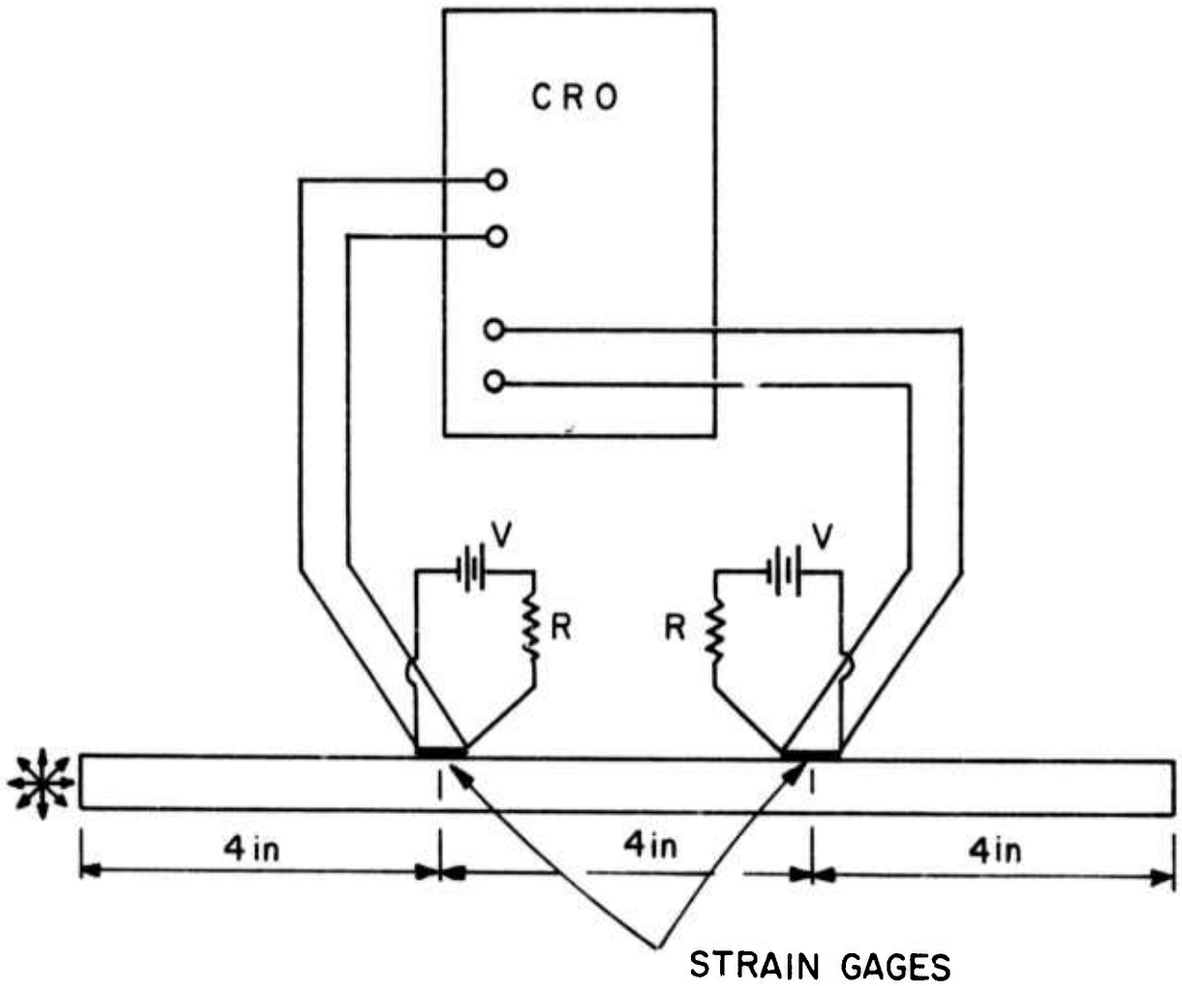

Fig. 12 SCHEMATIC OF INSTRUMENTATION FOR UNIAXIAL WAVE PROPAGATION STUDIES

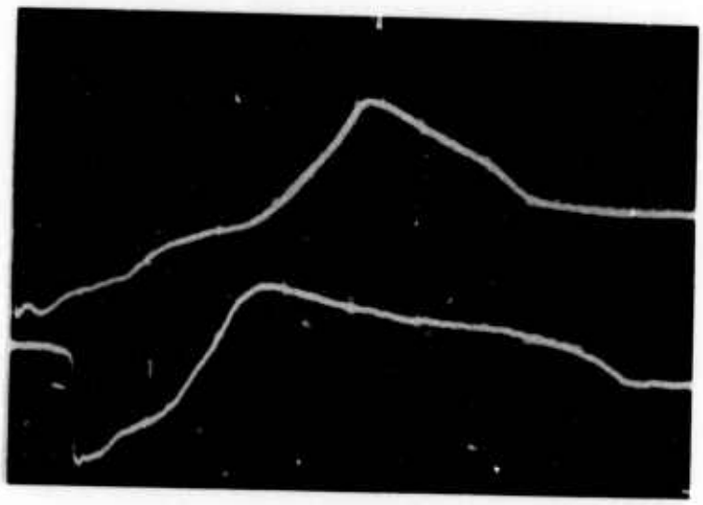

(a)

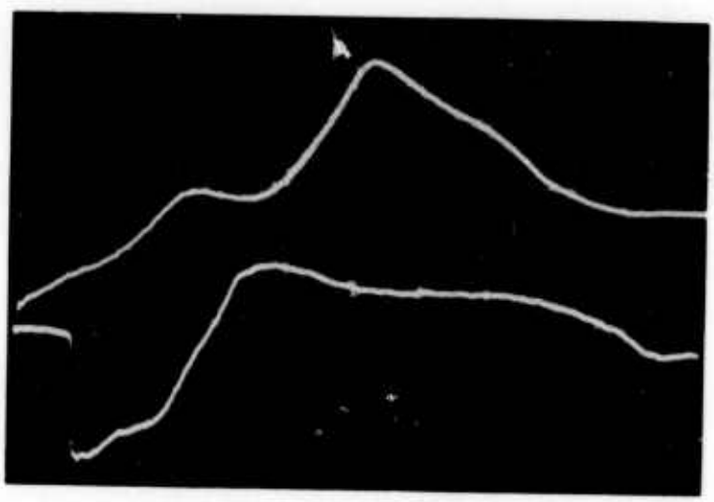

(b)

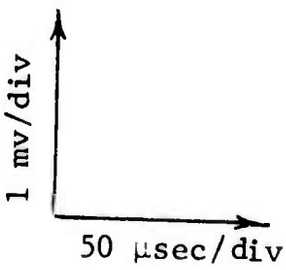

Fig. 13 STRAIN GAGE SIGNALS IN MARBLE BAR LOADED BY FALLING WEIGHT AT ONE END, (a) HEIGHT OF DROP 19 in., (b) HEIGHT OF DROP 38 in. (Upper Trace is First Gage 4 in. from Loaded End; Lower Trace is Second Gage 4 in. from First Gage)

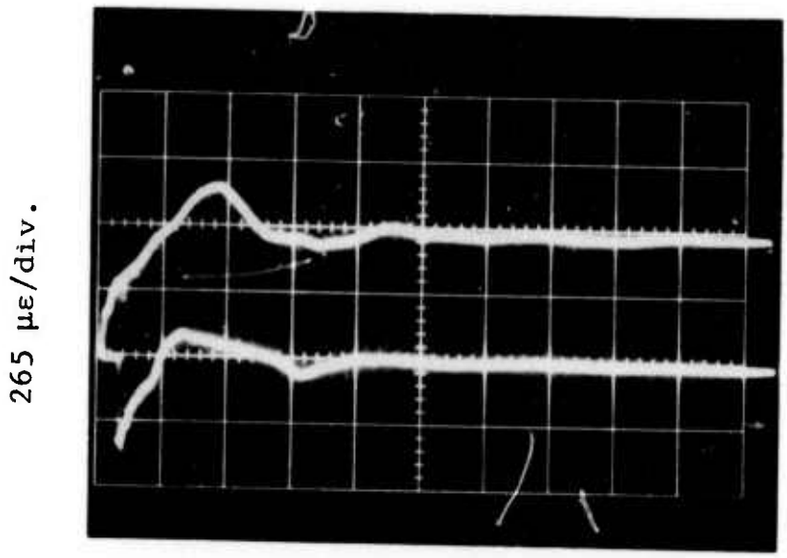

Fig. 14 STRAINS IN MARBLE BAR LOADED EXPLOSIVELY AT ONE END (UPPER TRACE IS FIRST GAGE 4 in. FROM LOADED END; LOWER TRACE IS SECOND GAGE 3.91 in. FROM FIRST GAGE AND 4 in. FROM UNLOADED END)

This was based on the time of travel of the compressive pulse between the two instrumented stations. Upon reflection from the free unloaded end the wave velocity decreased by approximately 50 percent. The dynamic modulus computed from Eq. (18) and a measured value for the density is

$$E = (155{,}000)^2 \ (250 \times 10^{-6}) = 6.0 \times 10^6 \text{ psi}$$

The reflected tensile pulse invariably fractured the specimen before reaching its peak value, thus this pulse has always a lower amplitude than the incident compressive pulse. Only the portion of the reflected tensile pulse which fractures the specimen is transmitted beyond the point of fracture. Thus, by measuring the amplitude of the tensile pulse transmitted beyond this point, one can determine the dynamic tensile strength of the material. The average of eight determinations of the dynamic tensile strength of marble was

$$\sigma_t = 2200 \text{ psi}$$

Figure 15 shows results from similar tests on granite bars. The average of four tests resulted in a uniaxial wave propagation velocity of

$$c_o = 210{,}000 \text{ in./sec}$$

Upon reflection from the free unloaded end the wave propagation velocity decreased by approximately 15 percent. The dynamic modulus computed from this velocity and the measured density of the material is

$$E = (210{,}000)^2 \ (246 \times 10^{-6}) = 10.8 \times 10^6 \text{ psi}$$

As in the case of marble, the reflected tensile pulse fractured the specimen in every case. The tensile strength measurements showed appreciable scatter due to the high inhomogeneity of the

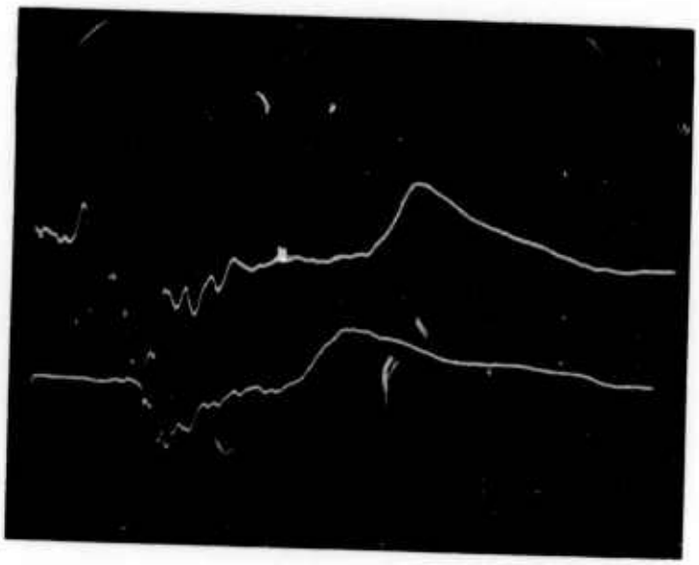

Fig. 15 STRAINS IN GRANITE BAR LOADED EXPLOSIVELY AT ONE END (UPPER TRACE IS FIRST GAGE AND LOWER TRACE IS SECOND GAGE; THE DISTANCES BETWEEN LOADED END, FIRST GAGE, SECOND GAGE AND UNLOADED END ARE 4 in., 3.75 in, AND 4 in., RESPECTIVELY)

material. The average dynamic tensile strength was

$$\sigma_t = 5500 \text{ psi}$$

5.2 Wave Propagation in Marble Plates

5.2.1 Photoelastic Coating Experiments

The specimens used in this study were 10 in. x 12 in. x 1/2 in. Vermont marble plates. These plates were coated with 0.080 in. thick photoelastic coatings and loaded on one edge with explosive charges between 100 mg and 400 mg (R. Stresau Laboratories, BM-9 and BM-2 detonators).

Photoelastic fringe patterns on the opaque rock specimens were recorded with a Beckman and Whitley camera type 189, operating at rates between 250,000 and 500,000 frames per second (Fig. 16). This camera is based on the Miller motion-compensation technique which eliminates the relative motion between the light rays reflected from a rotating mirror and the stationary film. The concept consists of a stationary objective lens, a rotating mirror, and one pair of stationary refocusing lenses for each frame. These refocusing lenses are located on arcs of a circle whose common center is the center of rotation of the mirror. A strip of stationary film is arranged along the arc of another circle, also with the mirror as center. The objective lens focuses a stationary primary image of say a fixed object onto or near the surface of the rotating mirror. When the reflected beam in its rotation passes over a typical refocusing lens pair, a stationary image is formed on the fixed film. Extremely fast shuttering is effected as the rotating mirror scans the light across successive pairs of refocusing lenses, thus producing multiple frames. The framing rate of cameras of this concept, as with that of a smear design, is directly proportional to the rotational speed of the mirror. This camera is capable of recording twenty-five 35mm frames at up to 2.5 million frames per second. Numerous light sources, such as ruby lasers, argon flash bombs, etc.,

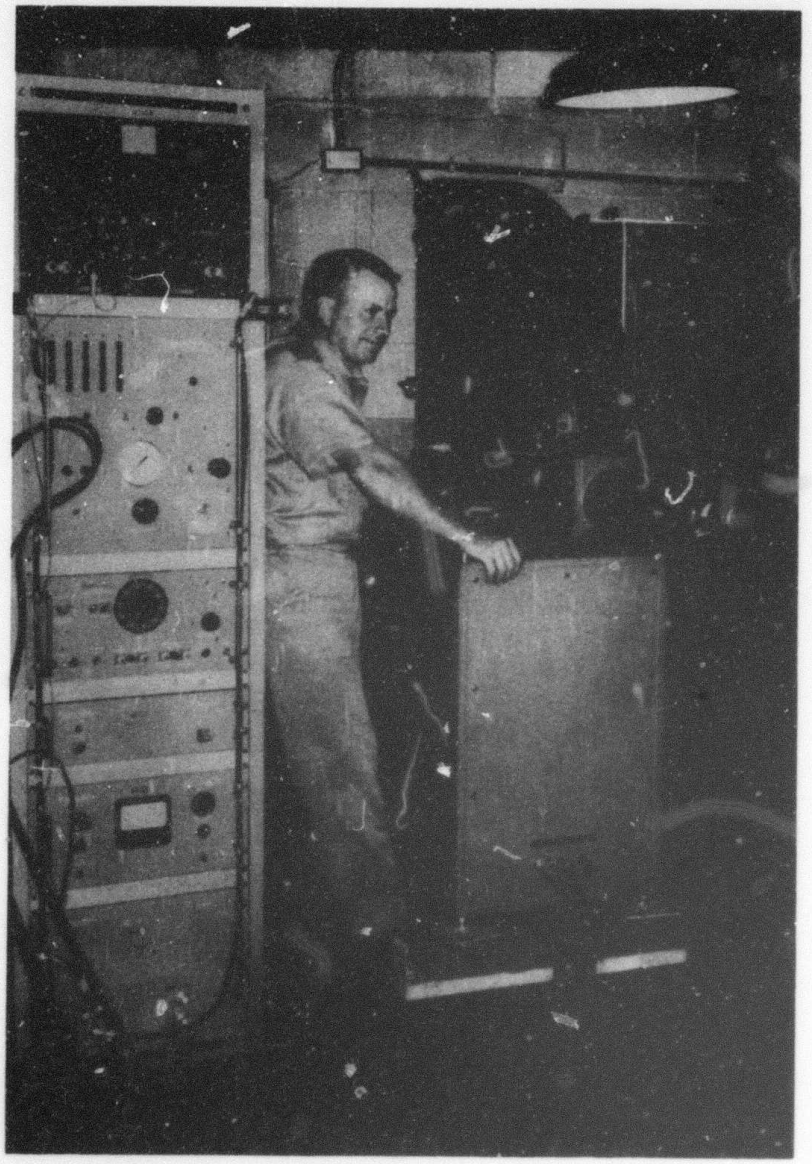

Fig. 16 BECKMAN AND WHITLEY MODEL 189 CAMERA

are available with this camera. Complete circuitry is provided for synchronizing camera, illumination and event. The model at IITRI has both framing and streak (or smear) capability. The conventional framing capability of such models has been used by Flynn[23] to record conventional dynamic photoelastic (transmission) fringe photographs. Cole[24] and associates have employed this type of camera on birefringent coatings to record (both in color and black and white) wave propagation in aluminum structures, while deGraf[25] used it to study fracture in steel. Bieniawski[3,16] has used a similar type of camera to study photoelastically fracture and crack propagation in rocks. Rowlands, Taylor and Daniel[26-27] have combined pulsed-laser illumination with the smear capability of the Beckman and Whitley type 189 to record photoelastically stress waves and fracture in polymeric materials.

The most critical problem in application of this camera was the light source. The applicability of the ruby laser was investigated, but the pulsed ruby laser available was not suitable for the application. Two other types of light source were used, the Argon bomb and an electronic flash. The Argon bomb used was a balloon approximately 12 in. in diameter and 36 in. long filled with Argon gas. This gas is ignited with an RP-1 detonator (Reynolds Industries, Inc.) and a 2 in. x 2 in. x 1/4 in. piece of Detasheet (E. I. DuPont and Company) detonated with a 2000 v pulse from the Beckman and Whitley camera. A Kodak gelatin filter No. 55 was used in front of the objective lens of the camera to isolate a band of light around the 5200 Angstrom wavelength.

Satisfactory isochromatic fringe patterns were obtained at 1,000,000 frames per second when one Argon bomb was used behind a transparent Plexiglas plate loaded with a detonator. However, the light from the Argon bomb was insufficient when reflected from the photoelastic coating applied to the rock specimen. To avoid complete destruction of the specimen the Argon bomb was directed at a mirror which reflected the light to the specimen.

In order to utilize more of the light it was attempted to record photoelastic coating fringe patterns in color by eliminating the monochromatic filter and by using high-speed color film (High-Speed Ektachrome film with 160 ASA rating, force-developed to 650 ASA and 1250 ASA). Although this approach produced visible fringe patterns, it is not the most preferred one because of the graininess of the film and the less than faithful reproduction of colors.

Another approach for utilizing more of the available light was considered by improving the reflectivity of the interface between the photoelastic coating and the rock specimen. In the usual applications, the photoelastic coatings are bonded to the specimen with an aluminum filled cement which provides a diffused reflective surface of low reflectivity. To improve the amount of reflected light, transparent photoelastic coatings were vacuum-deposited with aluminum to provide a mirror surface and were then bonded to the rock specimen with clear cement. Several tests were conducted with such specimens using the light of two Argon bombs reflected by a mirror, but the results were unsatisfactory.

A new light source was prepared for use with the Beckman and Whitley camera. It is an electronic flash unit employing a Xenon flash tube. It is similar to the Beckman and Whitley Model 357 flash unit incorporating some modifications proposed by Flynn.[28] It was found after several tests that the light produced by one flash tube was comparable to that of one Argon bomb and, therefore, inadequate. The possibility existed of adding more flash tubes to the system but was not pursued for financial reasons.

The effort was finally directed toward multiple Argon bombs aimed directly at the specimen. Photoelastic coatings with the usual aluminum filled cement were used. A variety of films and developers with varying development times were used. Films used were 4X developed in Acufine or D76 developer, Tri-X Pan developed in FG-7 developer, Kodak 2485 film developed in developer No. 857, and Double-X developed in Dektol.

Figure 17 shows one experimental setup used employing two Argon bombs located at a distance of 39 in. from the specimen off the centerline. Sixteen frames of a twenty-five frame record of isochromatic fringe patterns in the photoelastic coating on a marble specimen are shown in Fig. 18. The specimen was loaded on the edge with a BM-9 detonator (R. Stresau Laboratory; main charge 0.111 gm PETN, priming charge 0.110 gm Lead Azide). The camera was operated at a rate of 500,000 frames per second. The film used was 4X developed in Acufine developer. Figure 19 shows similar fringe patterns obtained with a marble specimen. In this case four Argon bombs were used as a light source. Tri-X Pan film developed in FG-7 developer was used.

Better results were obtained using Double-X film developed in Dektol developer for 4-1/2 minutes. Figures 20 and 21 show isochromatic fringe patterns for two marble specimens loaded with a BM-9 detonator. A similar marble specimen was loaded with a BM-2 detonator (R. Stresau Laboratory; main charge 0.331 gm PETN, priming charge 0.110 gm Lead Azide). The camera was operated at a rate of 250,000 frames per second. The purpose of this test was to span a longer, up to 100 μ sec, framing time and observe a later stage of the wave propagation phenomenon. Channel No. 1 of the camera was used to trigger the detonator and two Argon bombs 10 μ sec before frame No. 1. Channel No. 2 was delayed by 59 μ sec with respect to Channel No. 1 and was used to detonate two more Argon bombs. Figure 22 shows frames 16 through 23 of the record obtained.

The photoelastic records obtained were analyzed to determine wave propagation and attenuation characteristics. The propagation velocities of various fringe orders were measured and plotted versus fringe order and, by extrapolation to the zero order fringe, the wavefront velocity was obtained. Considerate scatter was observed in the results from many specimens. Values for the measured dilatational velocity ranged between 148,000 and 172,000 in./sec. Typical plots of propagation

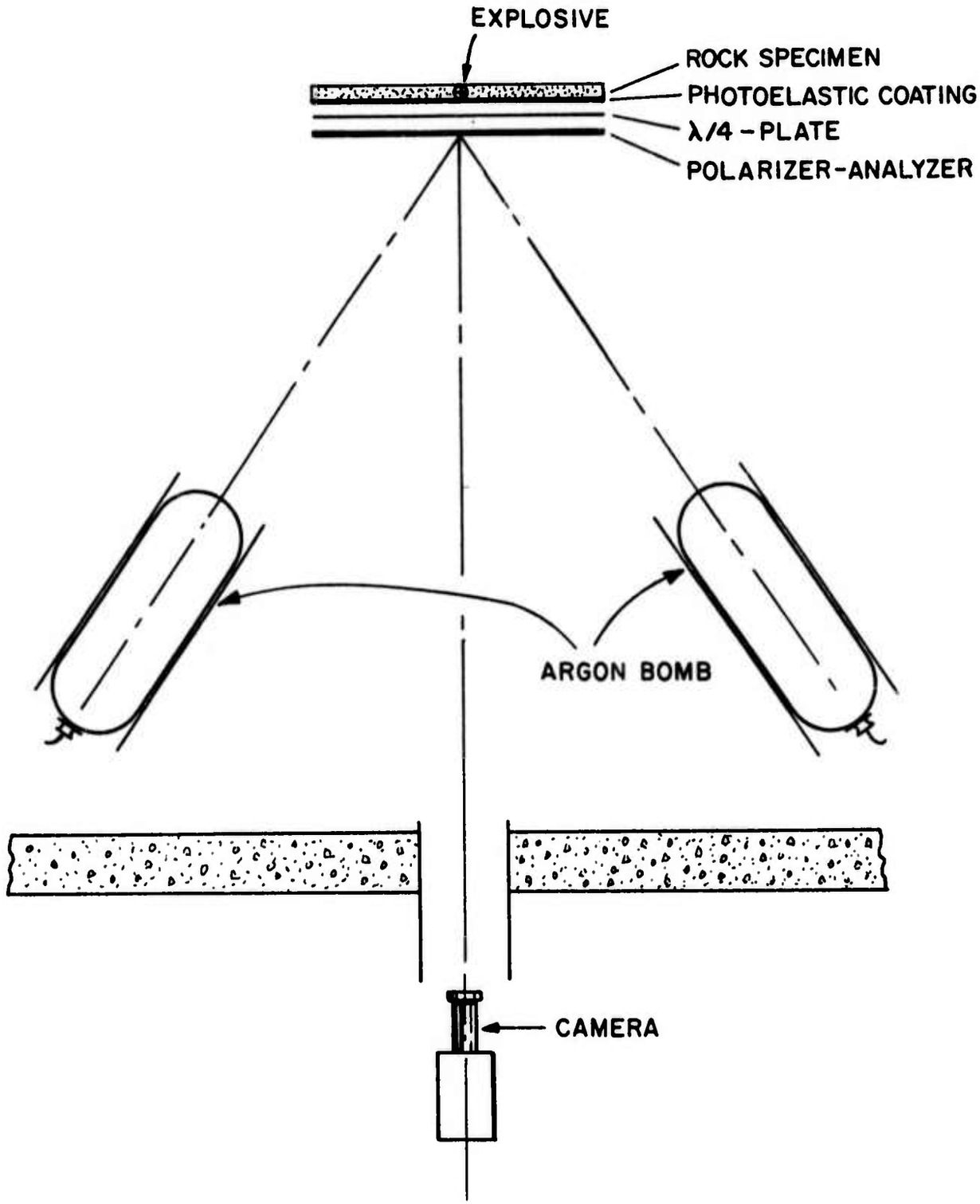

Fig. 17 EXPERIMENTAL SETUP FOR RECORDING ISOCHROMATIC FRINGE PATTERNS IN PHOTOELASTIC COATING ON ROCK SPECIMENS LOADED EXPLOSIVELY

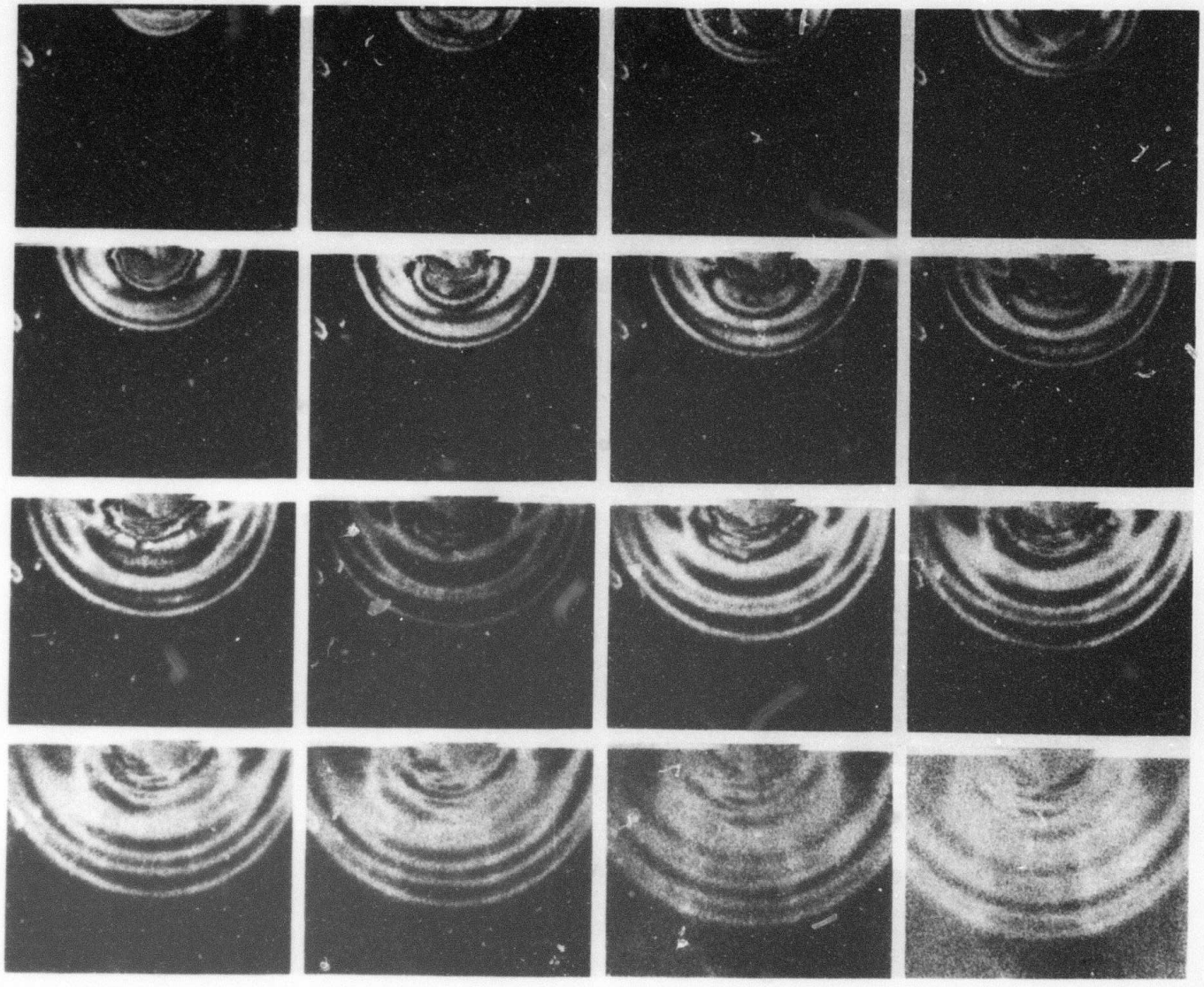

Fig. 18 ISOCHROMATIC FRINGE PATTERNS IN PHOTOELASTIC COATING ON MARBLE SPECIMEN LOADED EXPLOSIVELY ON THE EDGE. (CAMERA SPEED: 500,000 FRAMES PER SECOND; TIME RANGE: 14-44 μ SEC; SPECIMEN 100372-1)

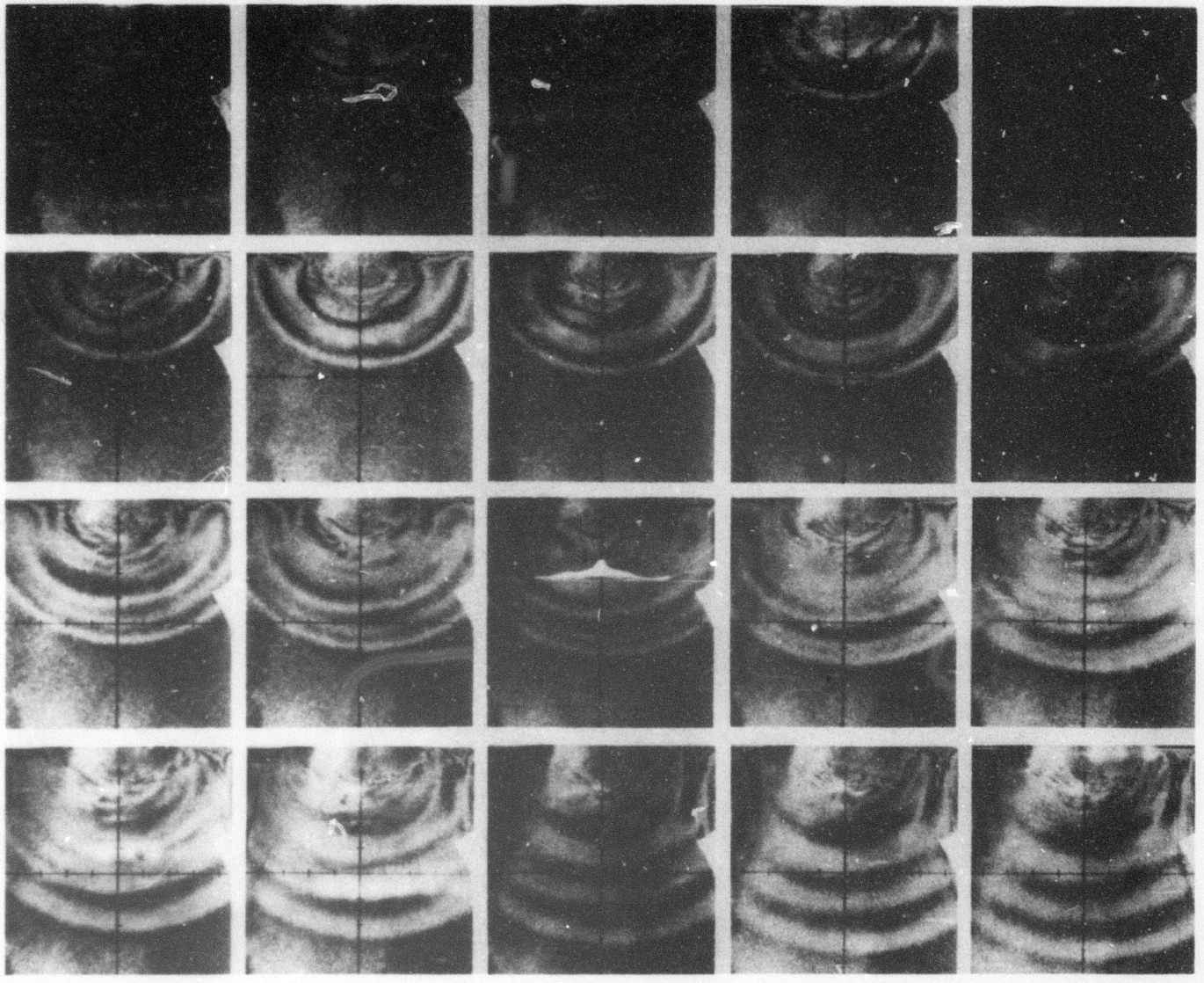

Fig. 19 ISOCHROMATIC FRINGE PATTERNS IN PHOTOELASTIC COATING ON MARBLE SPECIMEN LOADED EXPLOSIVELY ON THE EDGE. (CAMERA SPEED: 500,000 FRAMES PER SECOND; SPECIMEN 120172)

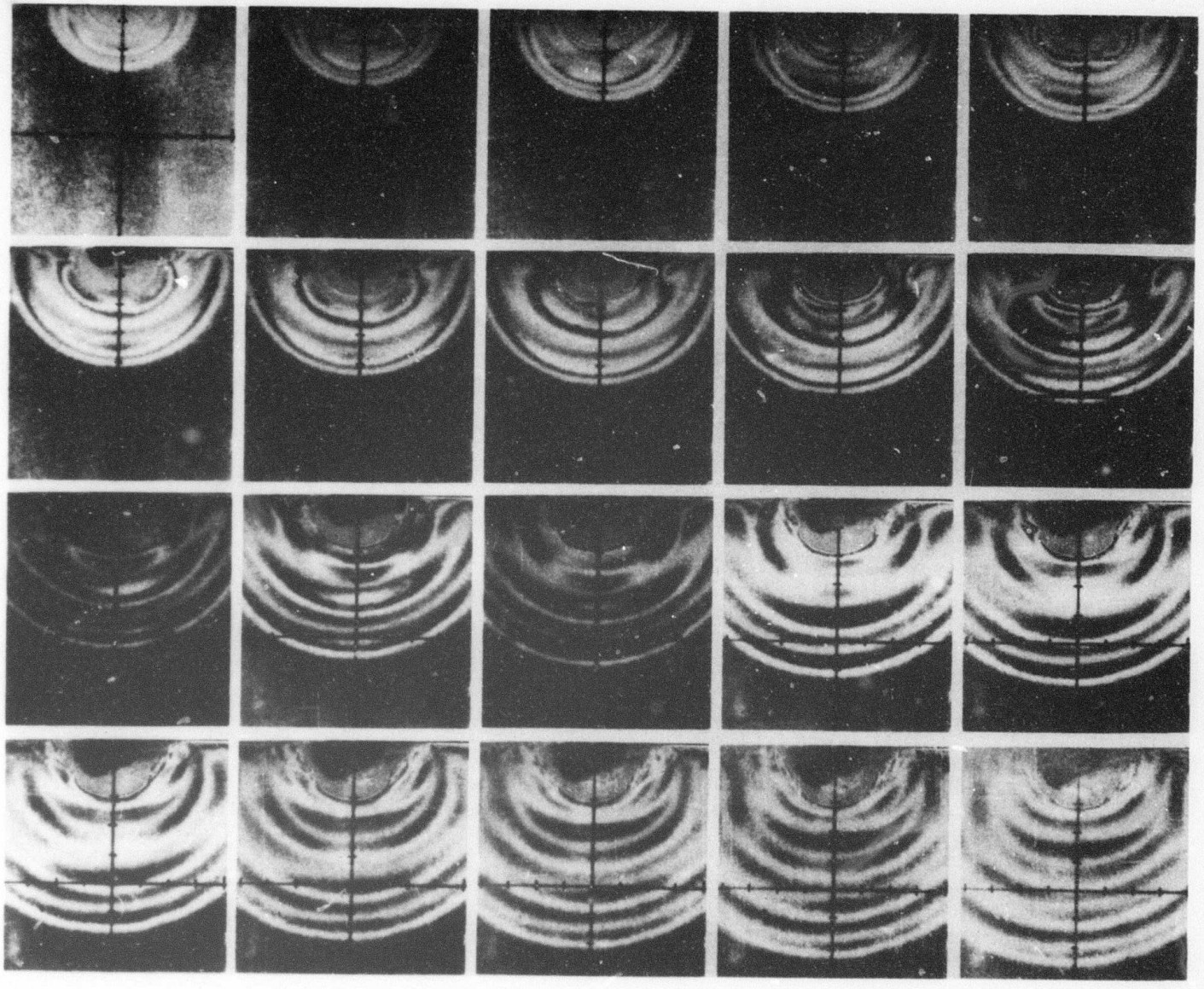

Fig. 20 ISOCHROMATIC FRINGE PATTERNS IN PHOTOELASTIC COATING ON MARBLE SPECIMEN LOADED EXPLOSIVELY ON THE EDGE. (CAMERA SPEED: 500,000 FRAMES PER SECOND; TIME RANGE: 18-56 μ SEC AFTER LOADING; SPECIMEN NO. 13173-1)

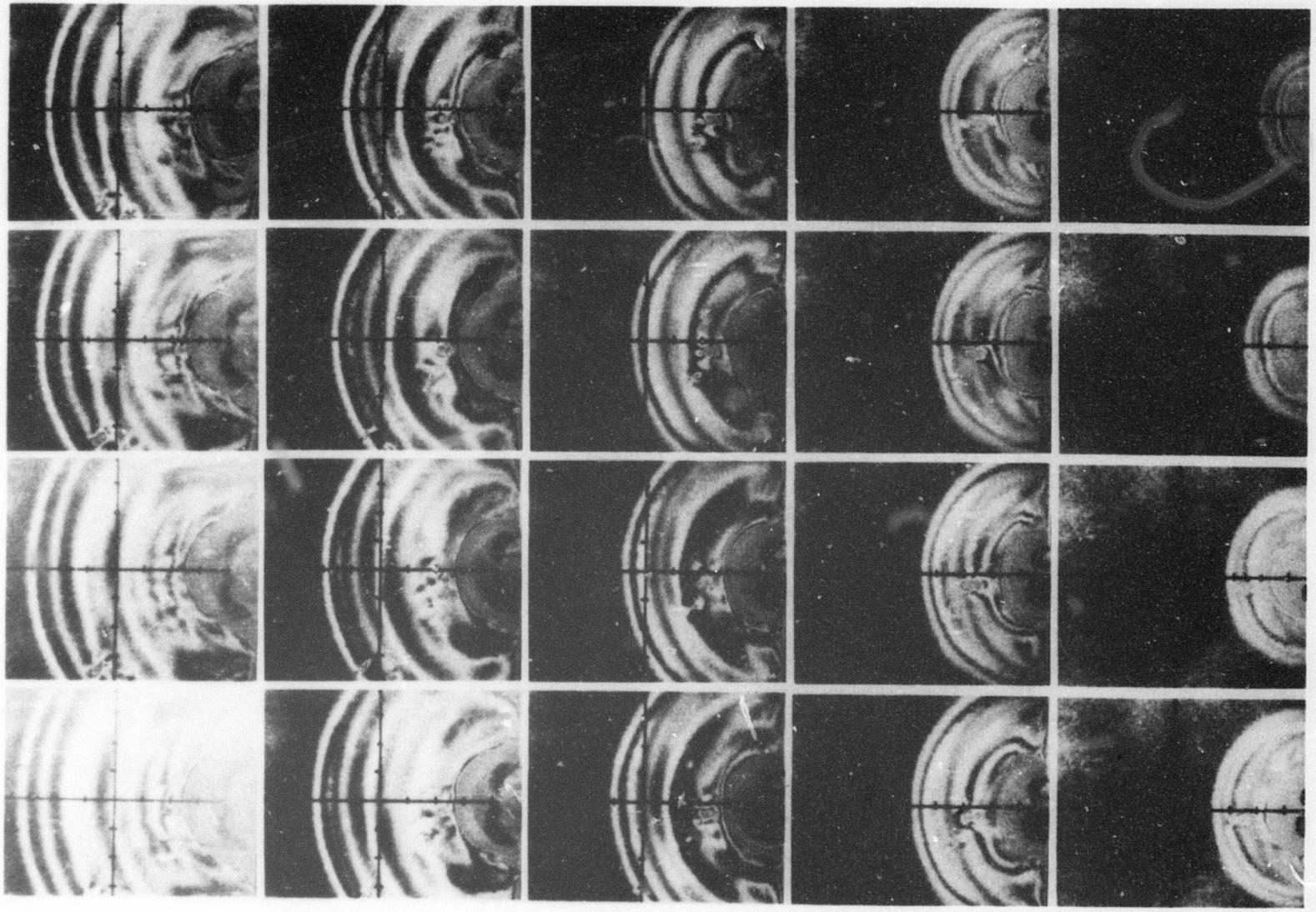

Fig. 21 ISOCHROMATIC FRINGE PATTERNS IN PHOTOELASTIC COATING ON MARBLE SPECIMEN LOADED EXPLOSIVELY ON THE EDGE. (CAMERA SPEED: 500,000 FRAMES PER SECOND; TIME RANGE: 16-54 μ SEC; SPECIMEN NO. 13173-2)

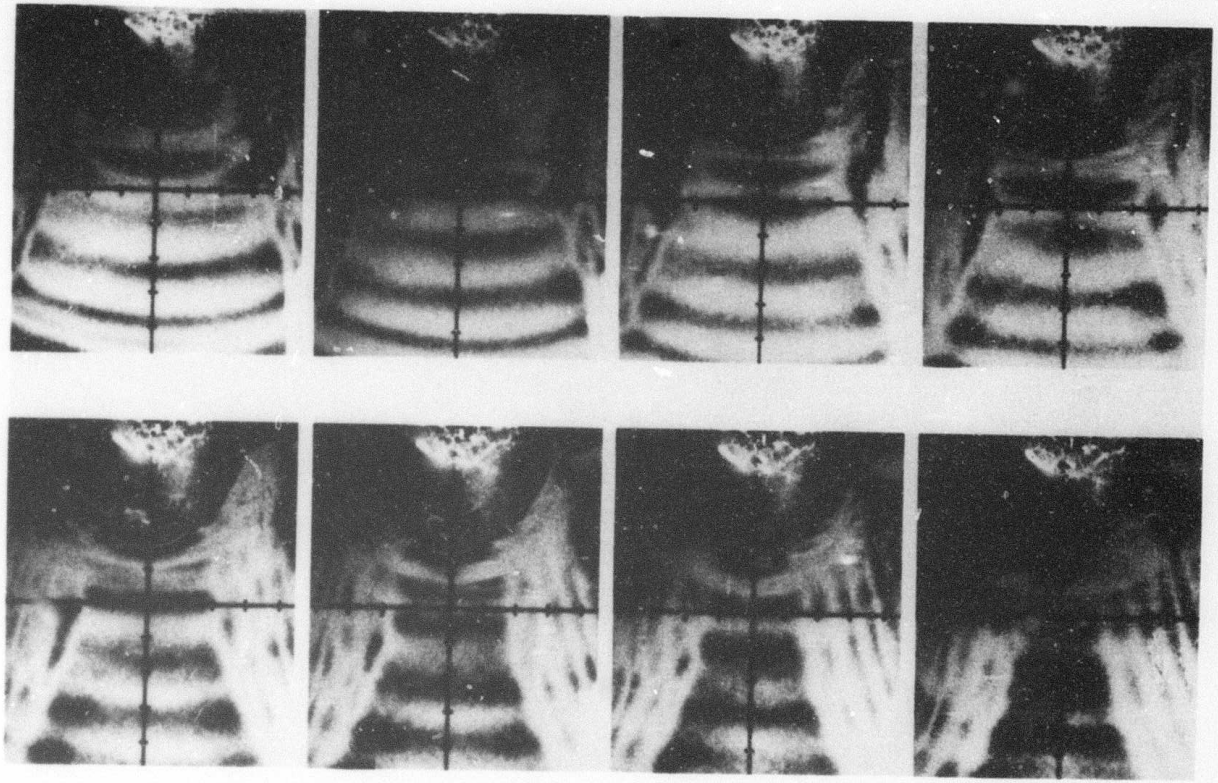

Fig. 22 ISOCHROMATIC FRINGE PATTERNS IN PHOTOELASTIC COATING ON MARBLE SPECIMEN LOADED EXPLOSIVELY ON THE EDGE. (CAMERA SPEED: 250,000 FRAMES PER SECOND; TIME RANGE: 70-98 μ SEC; SPECIMEN NO. 13173-3)

velocity versus fringe order are shown in Fig. 23 for four specimens.

In addition to the experiments above, marble plates were instrumented with strain gages and loaded on the edge with explosive charges (BM-9 detonators). From strain gage signals recorded on the oscilloscope a plate velocity of approximately 160,000 in./sec was determined.

The dilatational velocity in a plate under plane stress conditions is given by

$$c_L = \sqrt{\frac{E}{\rho(1-\nu^2)}} \tag{20}$$

Using the measured wave velocity of 155,000 in./sec in marble bars and a value for $\nu = 0.25$, the plate velocity is computed as $c_L = 161{,}000$ in./sec.

The shear wave propagation velocity was measured from the fringe patterns of Fig. 22. Because of the finite width of the plate the incident pulse is reflected from the free sides of the specimen. The most dominant reflected wave is the shear wave and is manifested in the form of nearly straight parallel fringes coming in from the sides of the specimen. The velocity of these fringes in the direction normal to them was measured and was found to remain nearly constant with fringe order. The measured shear wave propagation velocity was

$$c_s = 100{,}000 \text{ in./sec}$$

The shear wave velocity was also computed from the measured dilatational velocity and Poisson's ratio using relation (17):

$$c_s = c_L \sqrt{\frac{1-\nu}{2}} = 160{,}000 \sqrt{\frac{1-0.25}{2}} = 98{,}000 \text{ in./sec}$$

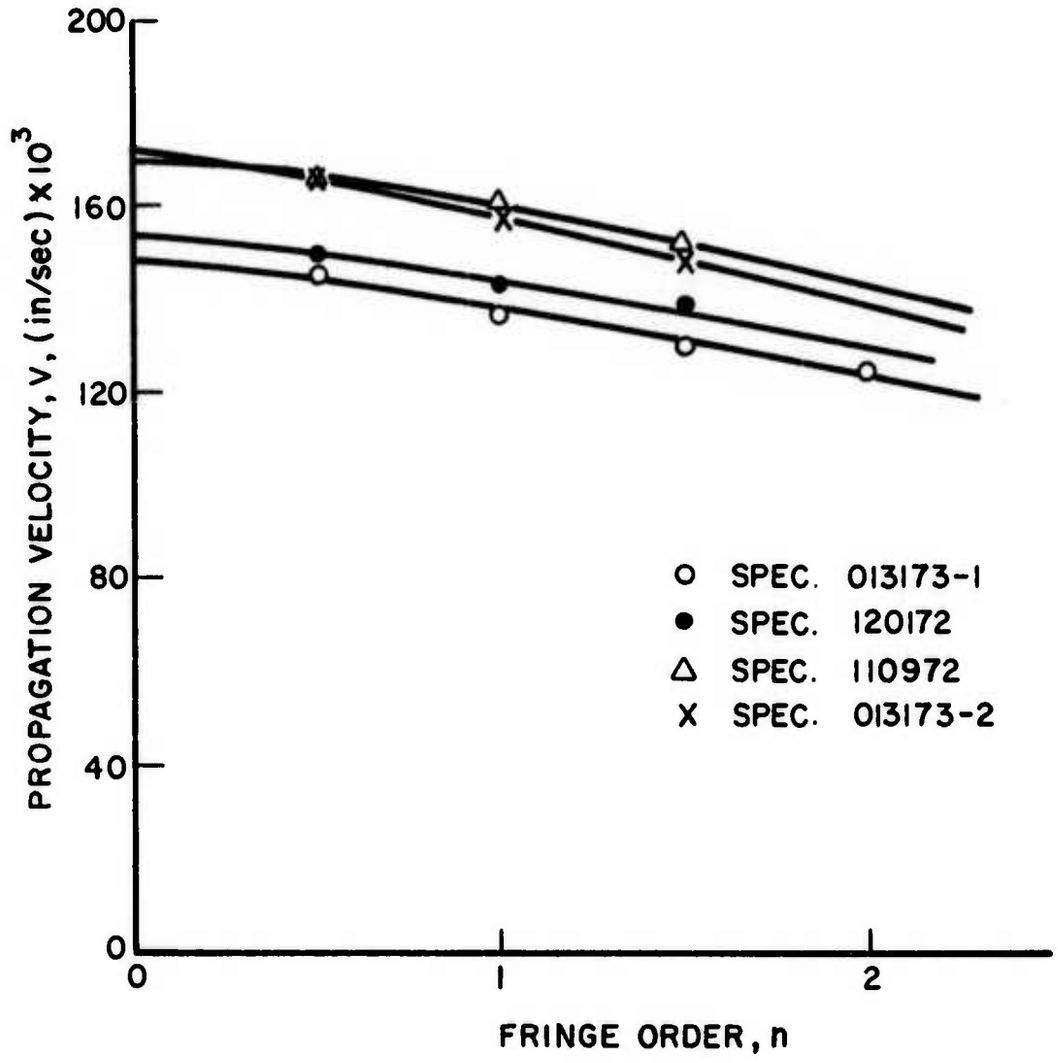

Fig. 23 WAVE PROPAGATION VELOCITY AS A FUNCTION OF FRINGE ORDER IN MARBLE PLATES

An attempt was made to identify a Rayleigh surface wave along the top edge of the specimen. An area of birefringence concentration on the edge can be discerned in the fringe patterns of Figs. 20 and 21. The propagation velocity of this pattern was measured to be 65,000 in./sec.

The fringe patterns of Fig. 20 were further analyzed to determine propagation and attenuation characteristics. Figure 24 shows the variation with time and distance of pulse shape and amplitude in terms of fringe order. The pulse has an undulating shape and the primary leading compressive pulse shows appreciable attenuation but without much noticeable dispersion. To separate the effects of geometric and material attenuation, an expression of the form

$$n_{max} = \frac{n_o e^{-ky}}{\sqrt{y}} \qquad (21)$$

for the maximum fringe order was sought, where y is the distance from the loading source and k, the coefficient of attenuation. The term $y^{-1/2}$ accounts for geometric attenuation in a two-dimensional space (plate). The attenuation coefficient and the constant n_o were obtained by plotting $n_{max}\, y^{1/2}$ versus y on a semilog scale (Fig. 25). Thus, for the dilatational wave in Vermont marble, we have

$$n_{max} = \frac{4.78e^{-0.101y}}{\sqrt{y}}$$

The loss tangent of the material for a sinusoidal pulse of wavelength λ is related to the attenuation coefficient by

$$\tan \delta = \frac{k\lambda}{\pi} \qquad (22)$$

For the dilatational wave in marble the loss tangent is computed as

$$\tan \delta \cong \frac{0.101 \times 3}{\pi} = 0.096$$

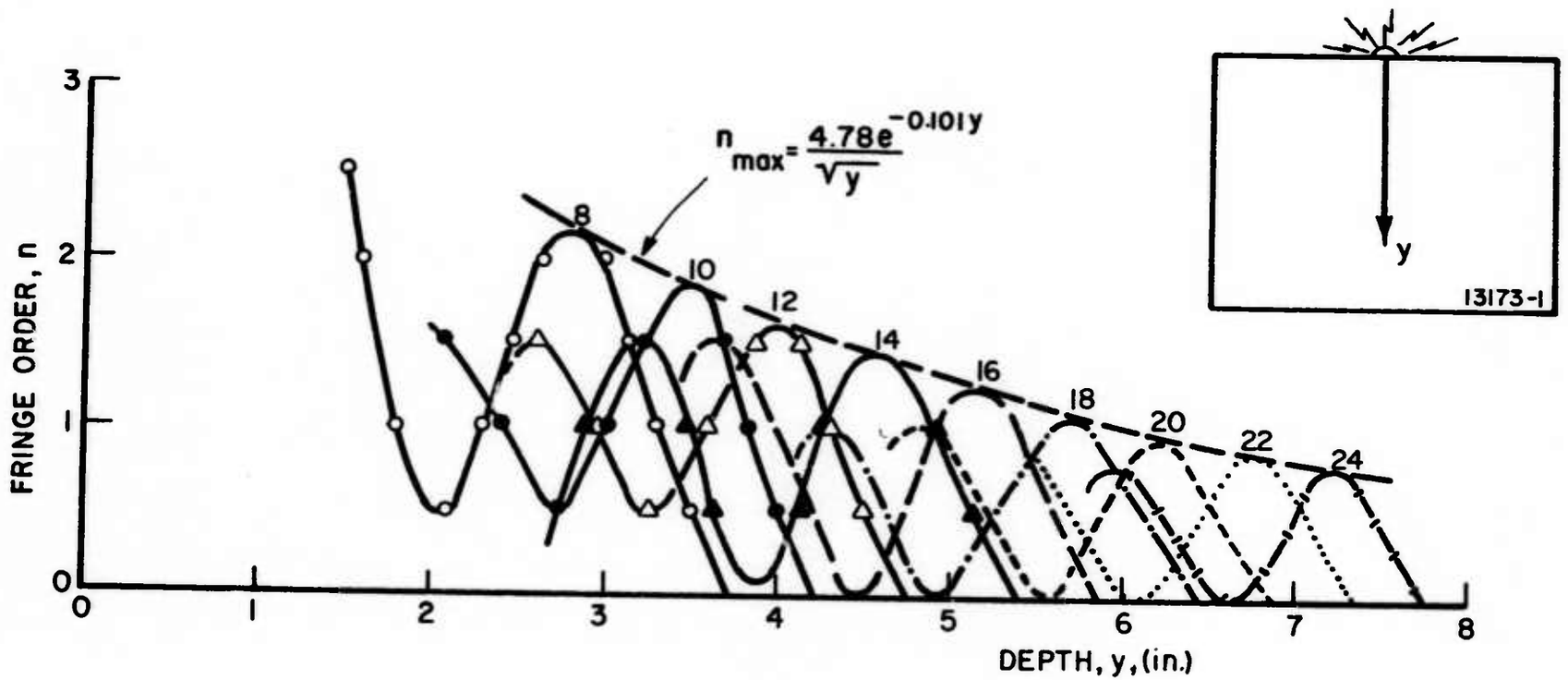

Fig. 24 FRINGE ORDER AS A FUNCTION OF LOCATION ALONG VERTICAL AXIS WITH TIME AS A PARAMETER (SPECIMEN 013173-1; FRAME NUMBERS ARE MARKED)

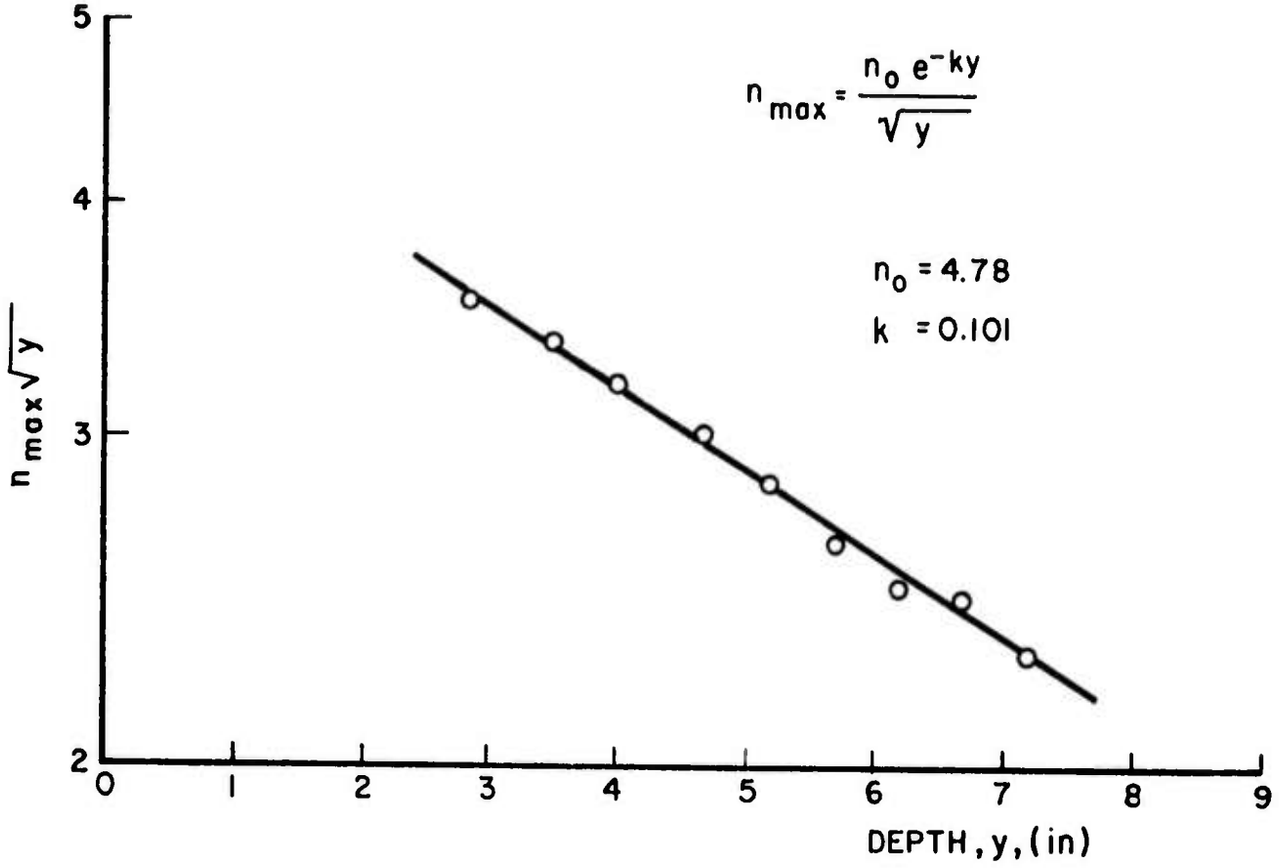

Fig. 25 SEMILOGARITHMIC PLOT FOR SEPARATING MATERIAL AND GEOMETRIC ATTENUATION

5.2.2. Moiré Experiments

Marble plates similar to those used in the photoelastic coating experiments were coated with 1000 line-per-inch rulings for application of moiré techniques. The specimen rulings were reproduced on 0.004 in. thick Kodaline reproduction film with estar base, and the film was bonded onto the specimen with the emulsion side outwards using an aluminum-filled cement (Photolastic PC-8 with PCH-8 hardener). The purpose of the aluminum filling was to provide a somewhat reflective interface for easier photography of fringe patterns. The specimen rulings were oriented parallel to the loaded edge of the specimen to yield full-field representation of the displacements normal to this edge. A film master with the same rulings was placed in contact and aligned with the specimen ruling by means of a film of oil.

The ruling density used, representing a practical upper limit for the current application, is not very sensitive with high modulus materials such as rock. To obtain an adequate analyzable response a higher explosive loading was used. This consisted of an RP-1 detonator (Reynolds Industries, Inc., 250 mg PETN initiating explosive, 385 mg Tetryl high density explosive and 4.1 gm RDX booster explosive), and two 3/4 in. diameter tetryl pellets placed under the first detonator. A small 3/16 in. thick steel plate was placed between the pellets and the specimen. Illumination was provided with two Argon bombs placed at distances between 25 in. and 32 in. from the specimens. Moiré fringe patterns during wave propagation were photographed with the Beckman and Whitley camera at rates between 500,000 and 1,000,000 frames per second. Doule-X film developed in Dektol or D-76 developer was used.

Figure 26 shows moiré fringe patterns in a marble specimen loaded with an RP-1 detonator and two tetryl pellets through a 3/16 in. steel plate. The two Argon bombs were placed at a distance of 32 in. from the specimen. The camera was operated at a rate of 1,004,500 frames per second. Figure 27 shows

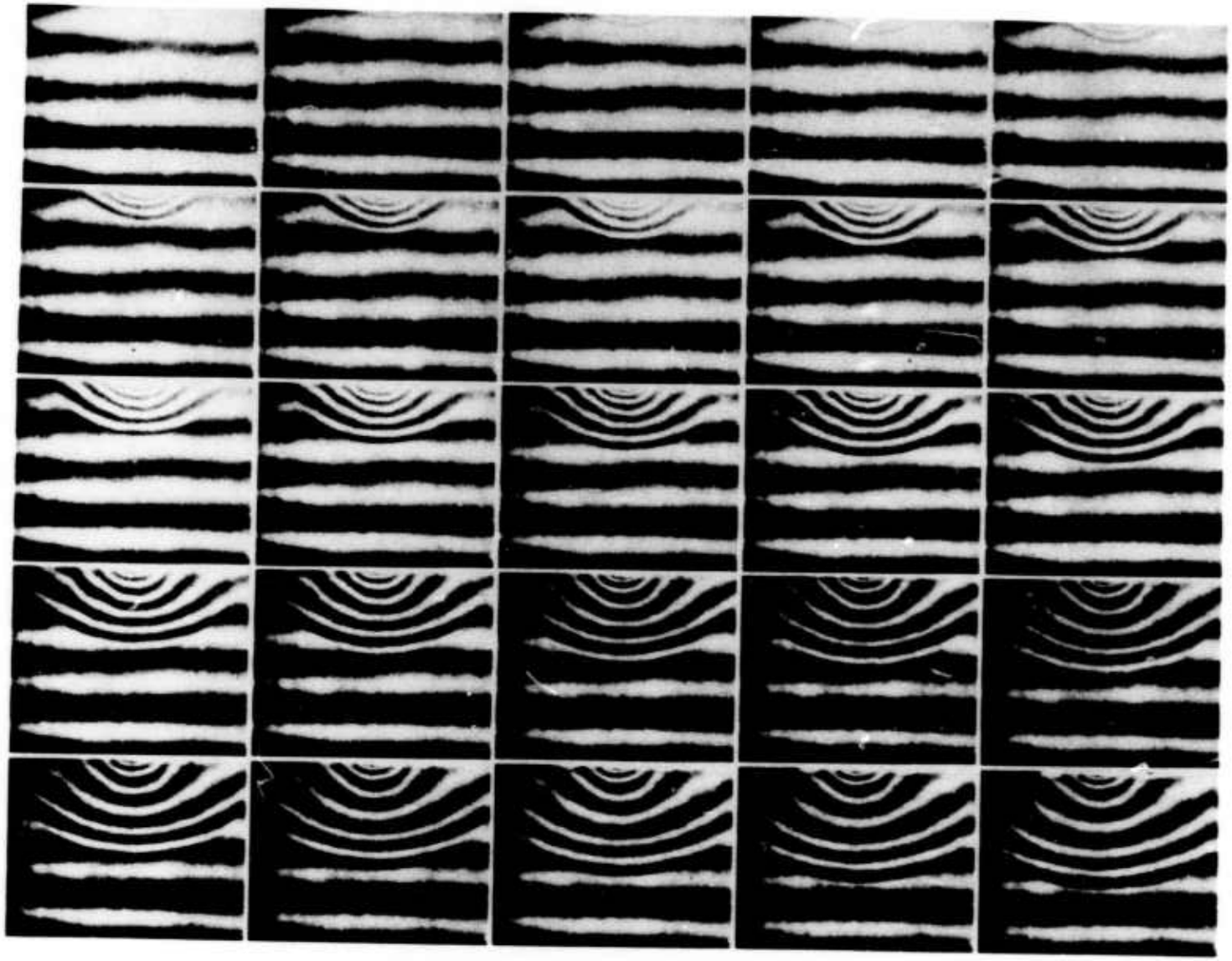

Fig. 26 MOIRÉ FRINGE PATTERNS CORRESPONDING TO VERTICAL DISPLACEMENTS IN MARBLE SPECIMEN LOADED EXPLOSIVELY ON THE EDGE (CAMERA SPEED: 1,004,500 FRAMES PER SECOND; RULING: 1,000 LINES PER INCH; SPECIMEN 41673-2)

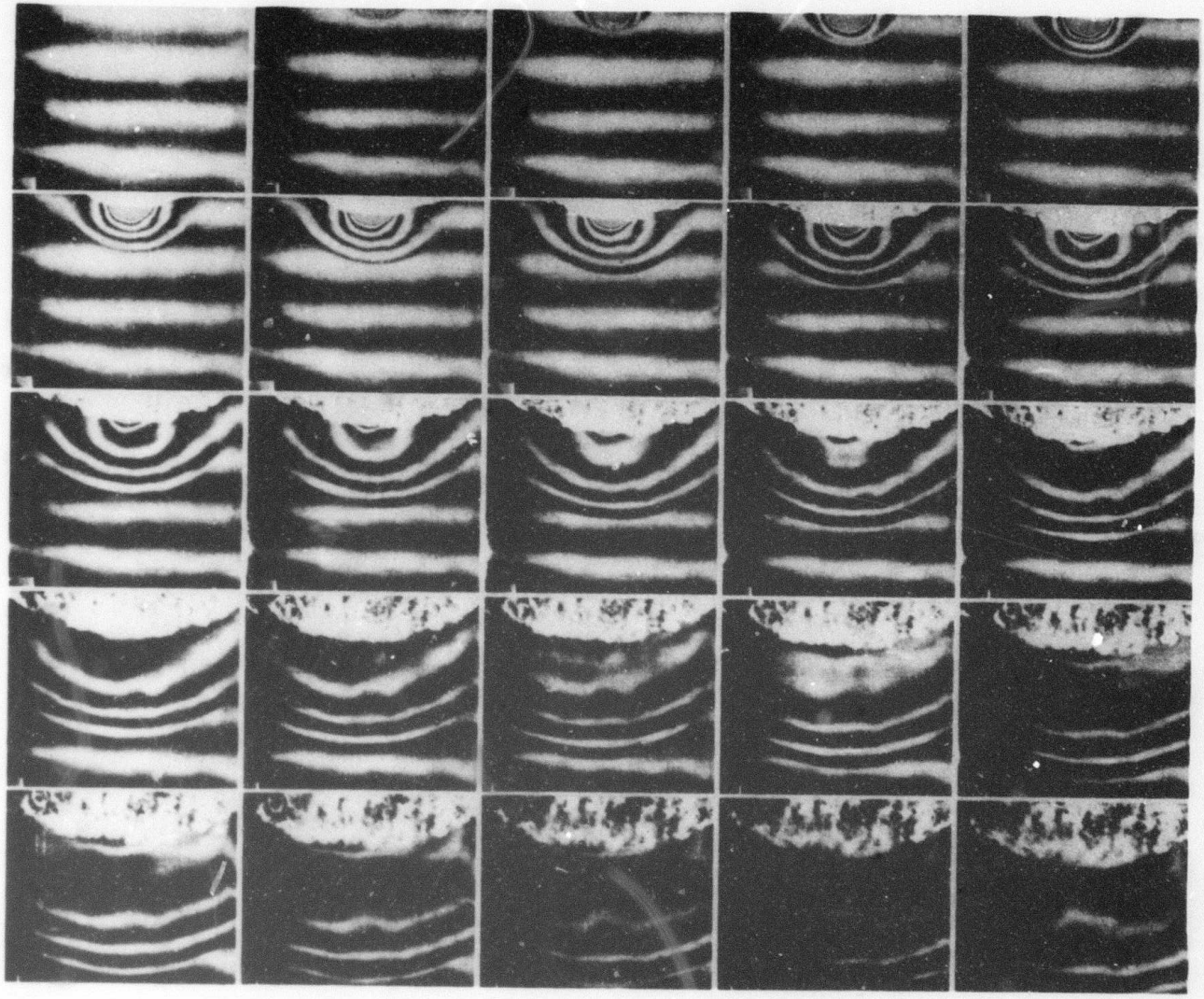

Fig. 27 MOIRÉ FRINGE PATTERNS CORRESPONDING TO VERTICAL DISPLACEMENTS IN MARBLE SPECIMEN LOADED EXPLOSIVELY ON THE EDGE (CAMERA SPEED: 508,000 FRAMES PER SECOND; RULING: 1,000 LINES PER INCH; SPECIMEN: 41673-3)

similar moiré patterns for a similarly loaded marble specimen. The Argon bombs were placed at a distance of 25 in. from the specimen and the camera was operated at a rate of 508,000 frames per second.

The moiré fringes obtained were interpreted and analyzed as loci of points having the same component of displacement normal to the ruling lines of the undistorted reference (master) array. Displacement profiles as a function of distance from the source for the two specimens above with time (or frame number) as a parameter are shown in Figs. 28 and 29. The attenuation and dispersion of the displacement pulse is evident. The pulse even shows sign reversal at later times (Frames 20-24 in Fig. 29).

The vertical displacements above are sufficient for the complete determination of stresses along the vertical centerline for the case of a dilatational wave. The strains along the y-axis are related to the displacements as follows:

$$\varepsilon_y = \frac{\partial v}{\partial y}$$

$$\varepsilon_x = \frac{v}{y} \qquad (23)$$

from which the stresses σ_x and σ_y can be determined. The vertical strains determined from the displacements of Fig. 29 are plotted in Fig. 30 as a function of distance from the source with time as a parameter. It is seen that the vertical strain becomes tensile at the trailing end of the pulse between frames 14 and 16. Since for the most part of the phenomenon the transverse strains are positive it follows that tensile stresses are generated at the trailing end of the pulse. Given the low tensile strength of rock, these tensile stresses are very likely to produce fracture.

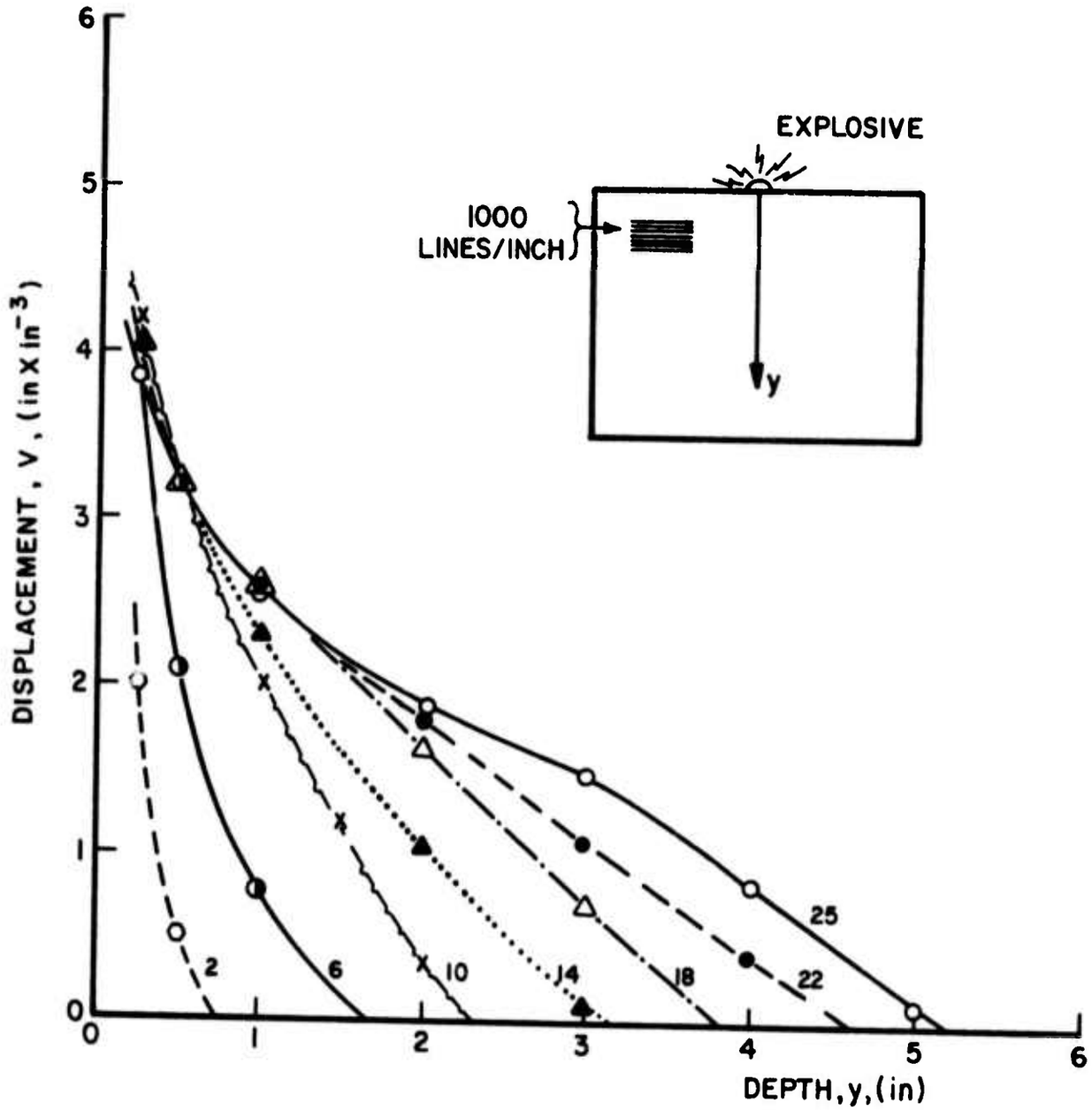

Fig. 28 VERTICAL DISPLACEMENT ALONG Y-AXIS AS A FUNCTION OF DEPTH WITH TIME AS A PARAMETER (FRAME NUMBERS MARKED; CAMERA SPEED: 1,004,500 FRAMES/SEC; MARBLE SPECIMEN 41673-2)

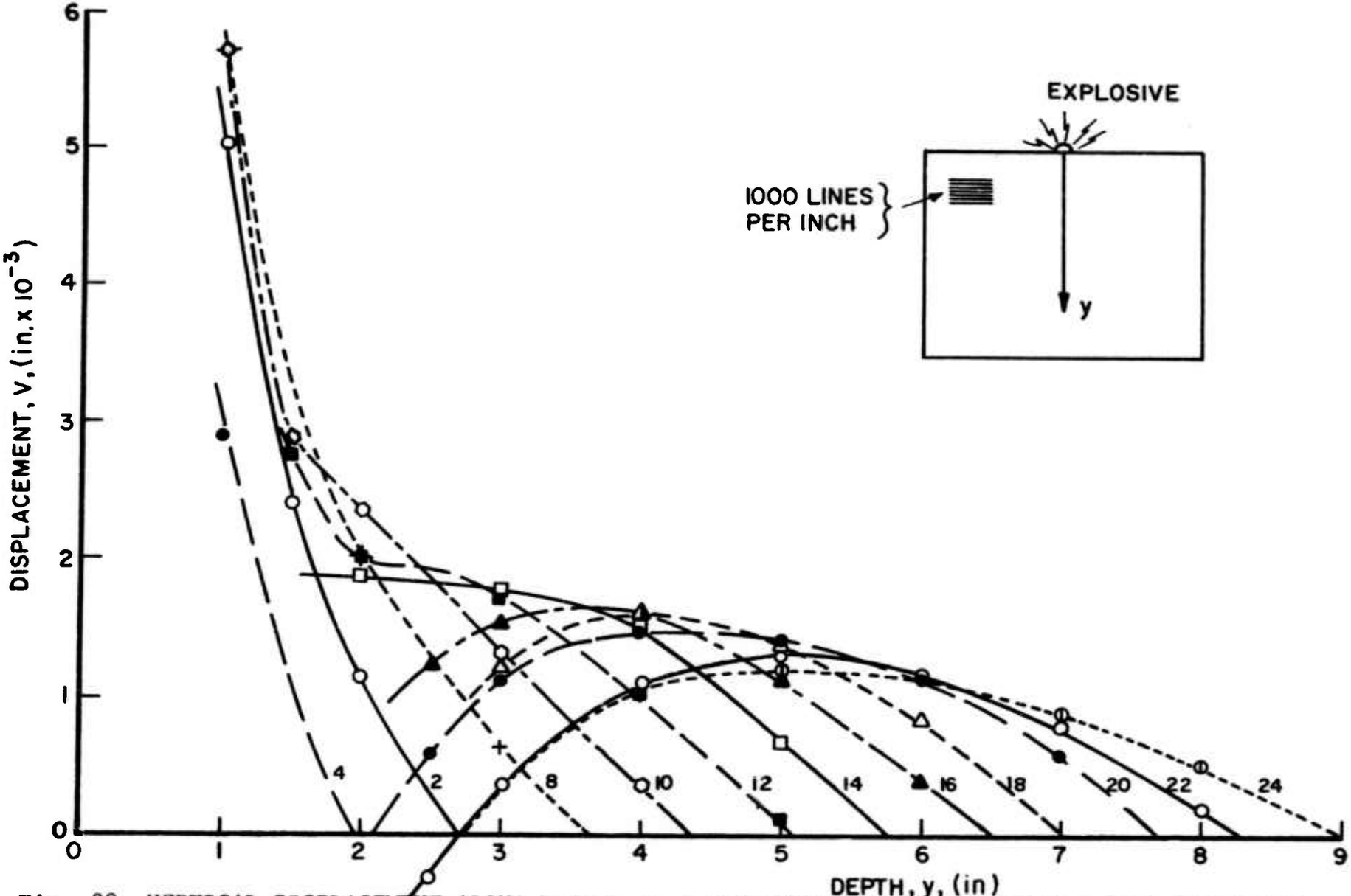

Fig. 29 VERTICAL DISPLACEMENT ALONG Y-AXIS AS A FUNCTION OF DEPTH WITH TIME AS A PARAMETER (FRAME NUMBERS MARKED; CAMERA SPEED: 508,000 FRAMES/SEC; MARBLE SPECIMEN 41673-3)

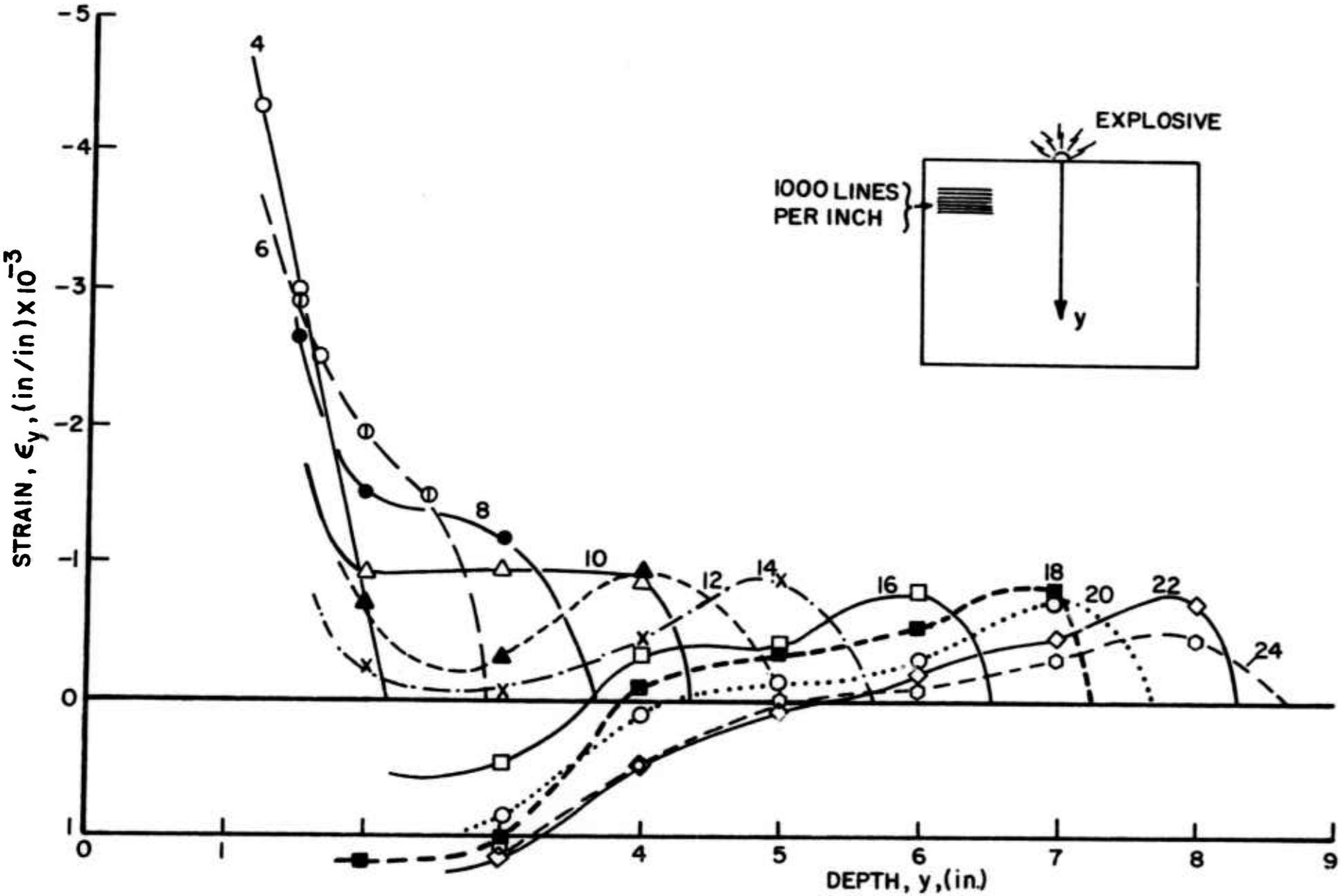

Fig. 30 VERTICAL STRAIN AS A FUNCTION OF DEPTH WITH TIME AS A PARAMETER (FRAME NUMBERS MARKED; CAMERA SPEED: 508,000 FRAMES/SEC; MARBLE SPECIMEN 41673-3)

5.3 Wave Propagation in Granite Plates

The specimens used were 10 in. x 12 in. x 1/2 in. Cold Spring (Minnesota) granite plates. They were coated with 0.080 in. thick photoelastic coatings. They were loaded explosively on one edge and the resulting isochromatic fringe patterns photographed with the Beckman and Whitley camera operating at a rate of 500,000 frames per second.

Figure 31 shows fringe patterns obtained from one granite specimen loaded with a BM-9 detonator. Two Argon bombs at a distance of 39 in. from the specimen were used as a light source. 4X film was used and developed in Acufine developer. Figure 32 shows similar fringe patterns obtained from a similar granite specimen loaded with a BM-2 detonator on the edge. Three Argon bombs placed at a distance of 36 in. from the specimen were used as the light source. Double-X film processed in Dektol developer was used. The fringe patterns in both cases are not well defined because of the pronounced inhomogeneity of granite. The material seems to consist of large grains of varying mechanical and thermal properties. Temperature changes from the temperature at which the coating was bonded induce nonuniform fringe patterns which are superimposed on the patterns induced by loading.

The wave propagation of various fringe orders was measured and plotted versus fringe order in Fig. 33. The dilatational wave propagation velocity obtained by extrapolation to the zero-order fringe was 172,000 and 192,000 in./sec for the two specimens. As in the case of marble appreciable attenuation is evident.

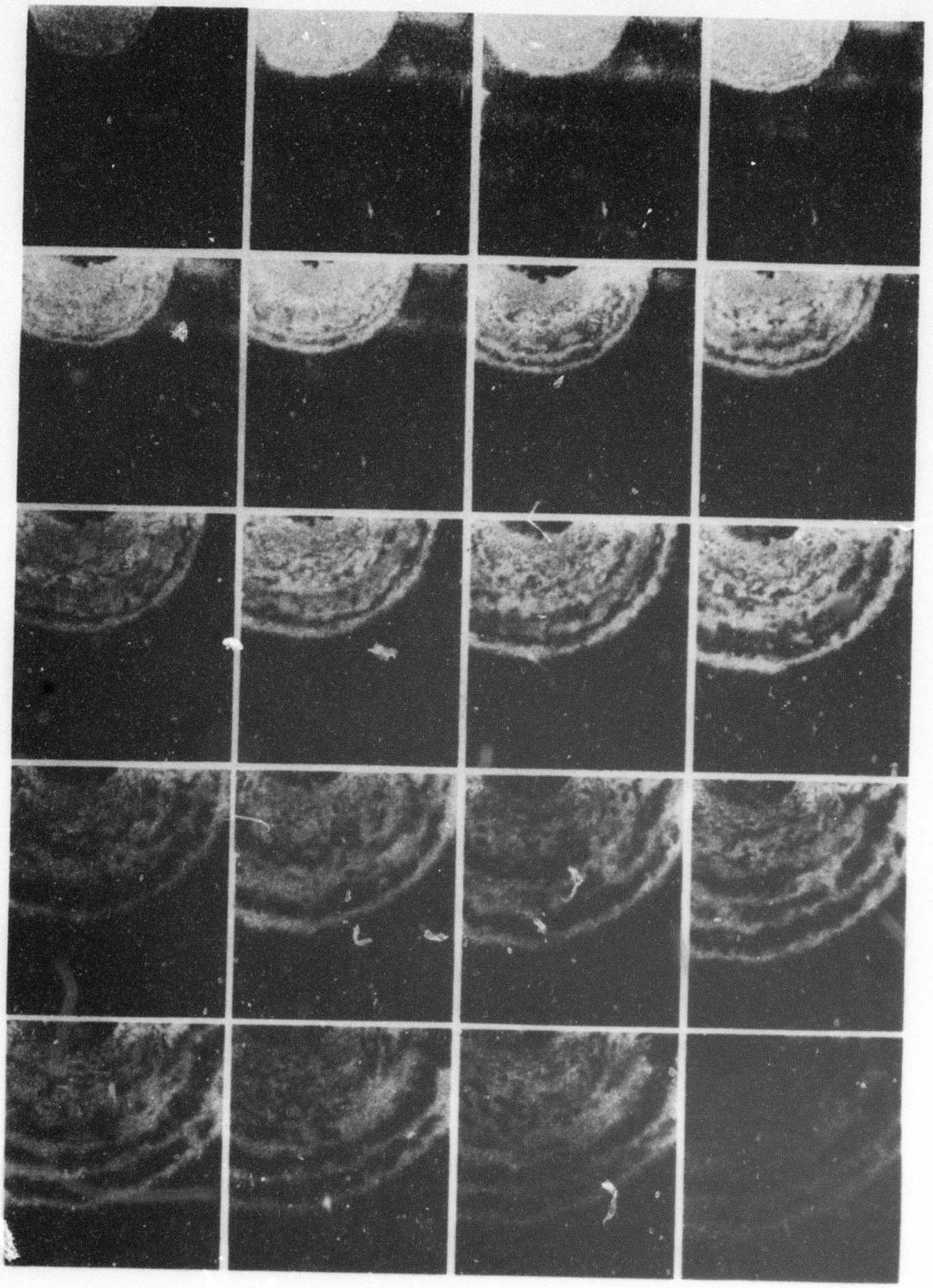

Fig. 31 ISOCHROMATIC FRINGE PATTERNS IN PHOTOELASTIC COATING ON GRANITE SPECIMEN LOADED EXPLOSIVELY ON THE EDGE (CAMERA SPEED: 500,000 FRAMES PER SECOND; TIME RANGE: 14-52 μ SEC; SPECIMEN 100372-2)

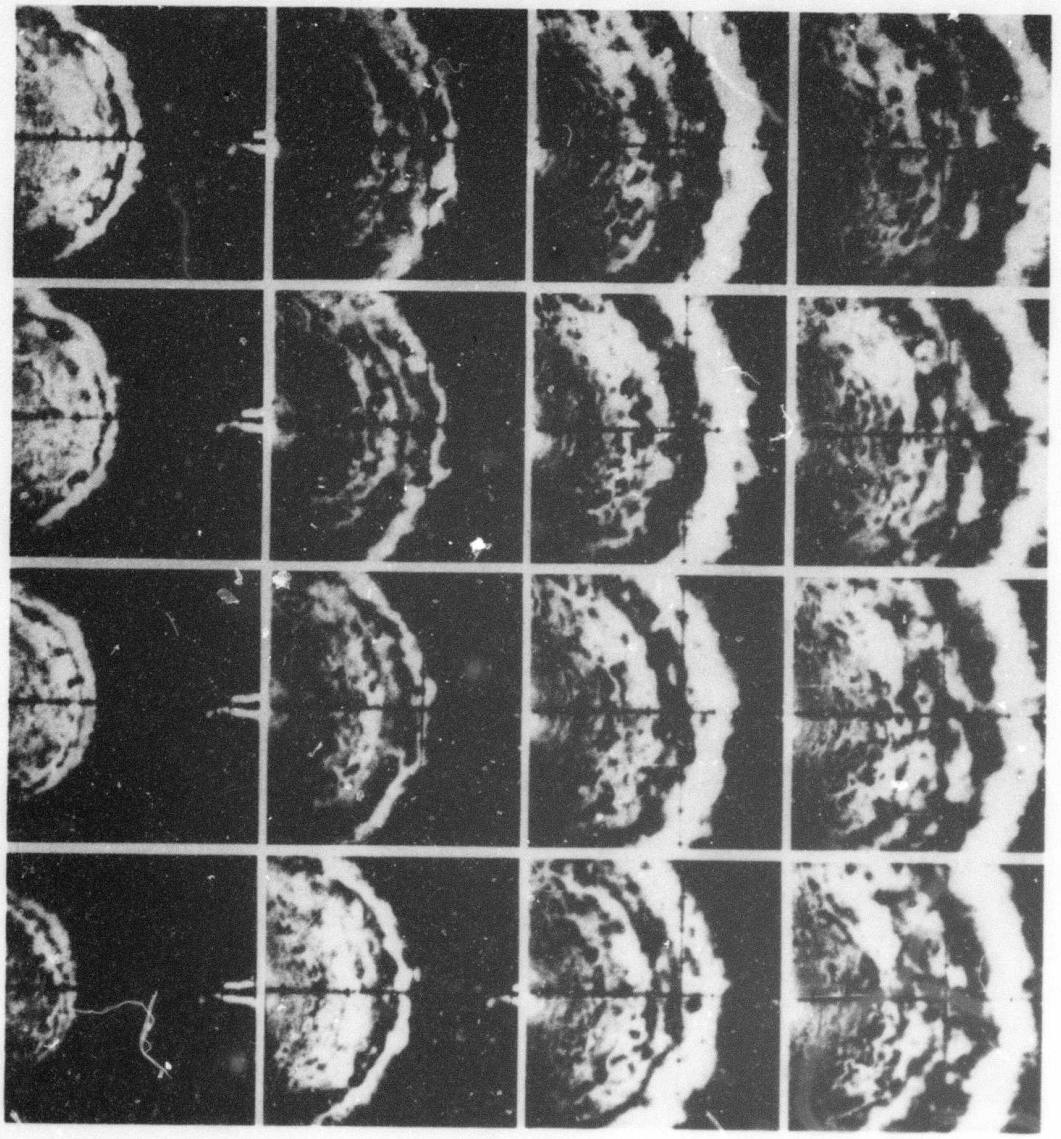

Fig. 32 ISOCHROMATIC FRINGE PATTERNS IN PHOTOELASTIC COATING ON GRANITE SPECIMEN LOADED EXPLOSIVELY ON THE EDGE (CAMERA SPEED: 500,000 FRAMES PER SECOND; TIME RANGE: 22-52 μ SEC; SPECIMEN 030173-2)

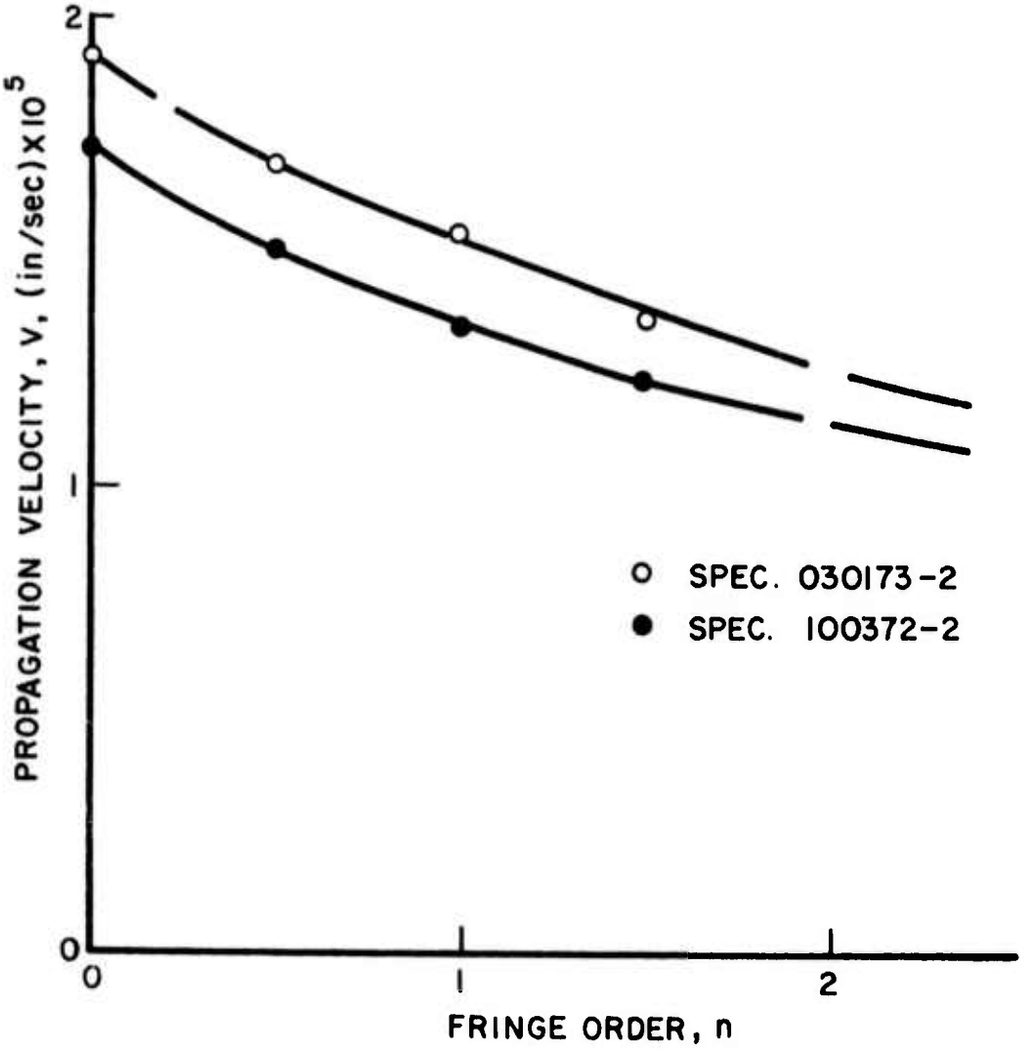

Fig. 33 WAVE PROPAGATION VELOCITY AS A FUNCTION OF FRINGE ORDER IN PHOTOELASTIC COATING ON GRANITE SPECIMENS

6.0 FRACTURE PROPAGATION IN ROCK MEDIA

It was shown earlier that the initially compressive pulse undergoes sign changes with tensile stresses developing at the trailing end at later times. If the initial pulse is sufficiently intense the geometric and material attenuation will not reduce these tensile stresses to a level below the tensile strength of the material. This phenomenon results in a fracture zone around the point source clearly evident as the nearly semicircular region of dense fringes in Figs. 20-22. The propagation velocity of the boundary of this zone was measured in the marble specimens of Figs. 20 and 21 as 30,000 and 35,000 in./sec. A similar fracture zone develops in granite specimens. These fractures are illustrated in Fig. 34 for marble and granite. In the case of the granite specimen additional fractures near the upper corners were caused by tensile pulses reflected from the sides of the specimen.

Several attempts were made to induce crack propagation in the rock plates. A notch was introduced at the bottom of the specimen opposite the loaded edge with the expectation that the tensile pulse reflected from the bottom edge would initiate a crack. This, however, did not occur, probably because of the high attenuation of the wave. A notch was then introduced at the upper edge and the specimens loaded with explosive packed inside this notch. Figure 35 shows isochromatic fringe patterns obtained from a marble specimen loaded explosively through a notch. An RP-1 detonator and 2.23 gm of Deta sheet were used. Four Argon bombs placed at a distance of 36 in. from the specimen were used as a light source. The film was Double-X developed in Dektol.

The propagation of the fracture zone identified as the area of dense fringe pattern was measured (Fig. 36). The velocity of propagation of the boundary of this zone is not uniform but a value of

$$v_{fracture} = 50{,}000 \text{ in./sec}$$

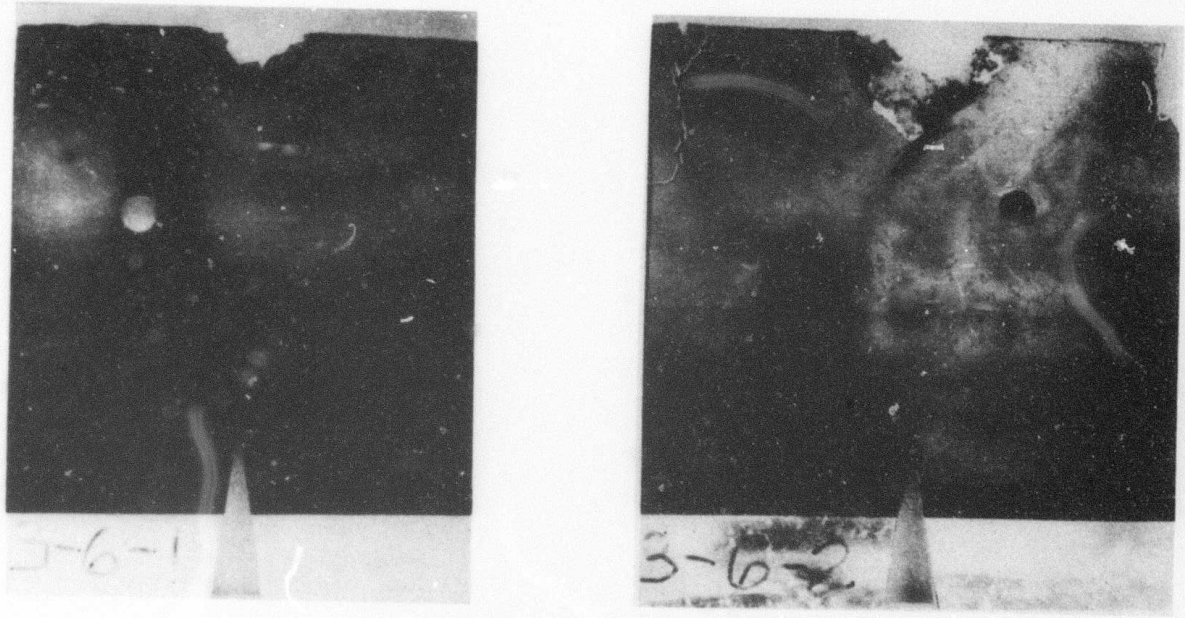

Fig. 34 MARBLE AND GRANITE SPECIMENS AFTER LOADING

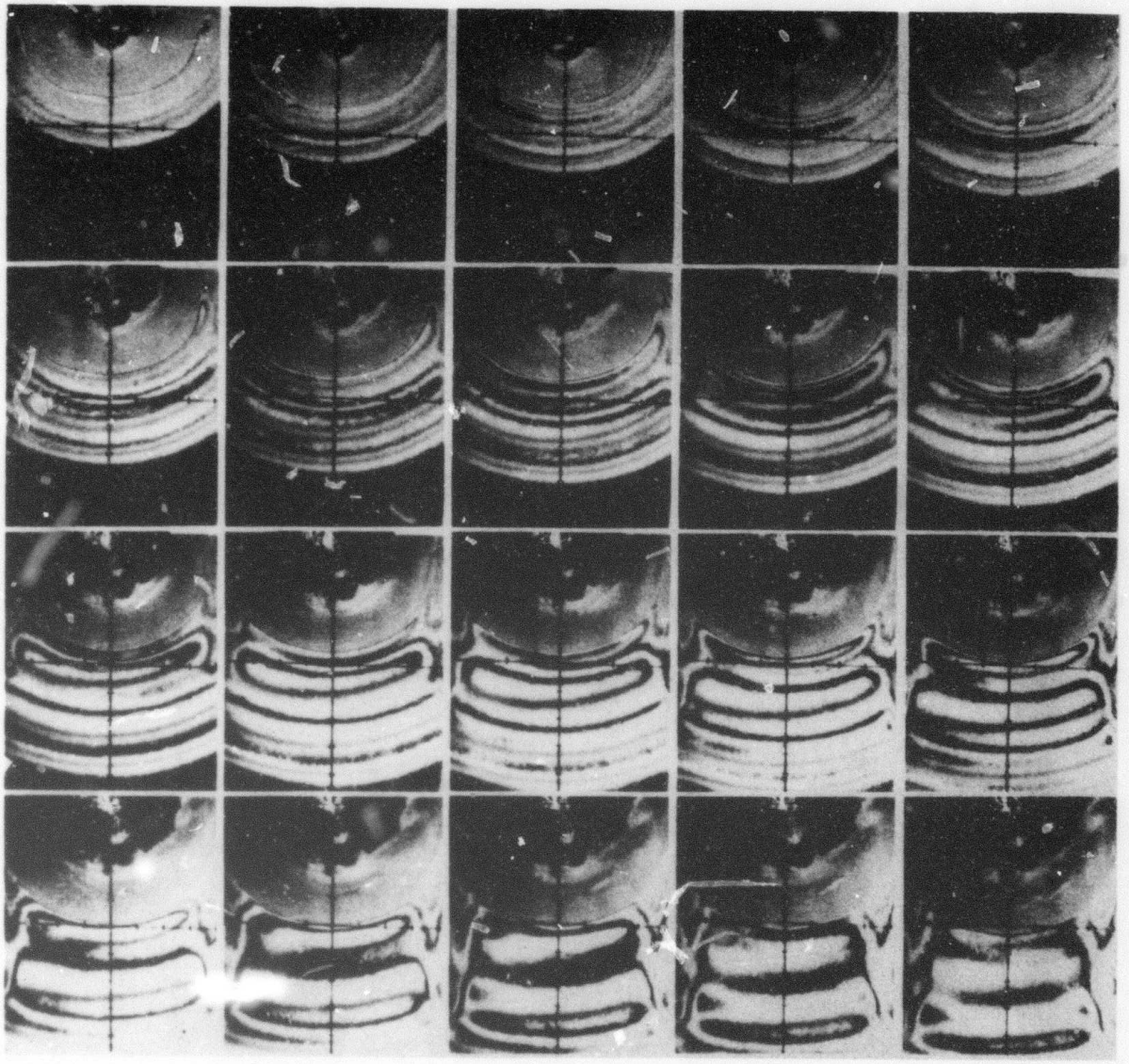

Fig. 35 ISOCHROMATIC FRINGE PATTERNS IN PHOTOELASTIC COATING ON MARBLE SPECIMEN LOADED EXPLOSIVELY THROUGH A NOTCH (CAMERA SPEED: 500,000 FRAMES PER SECOND; TIME RANGE: 32-70 μ SEC; SPECIMEN 20173-3)

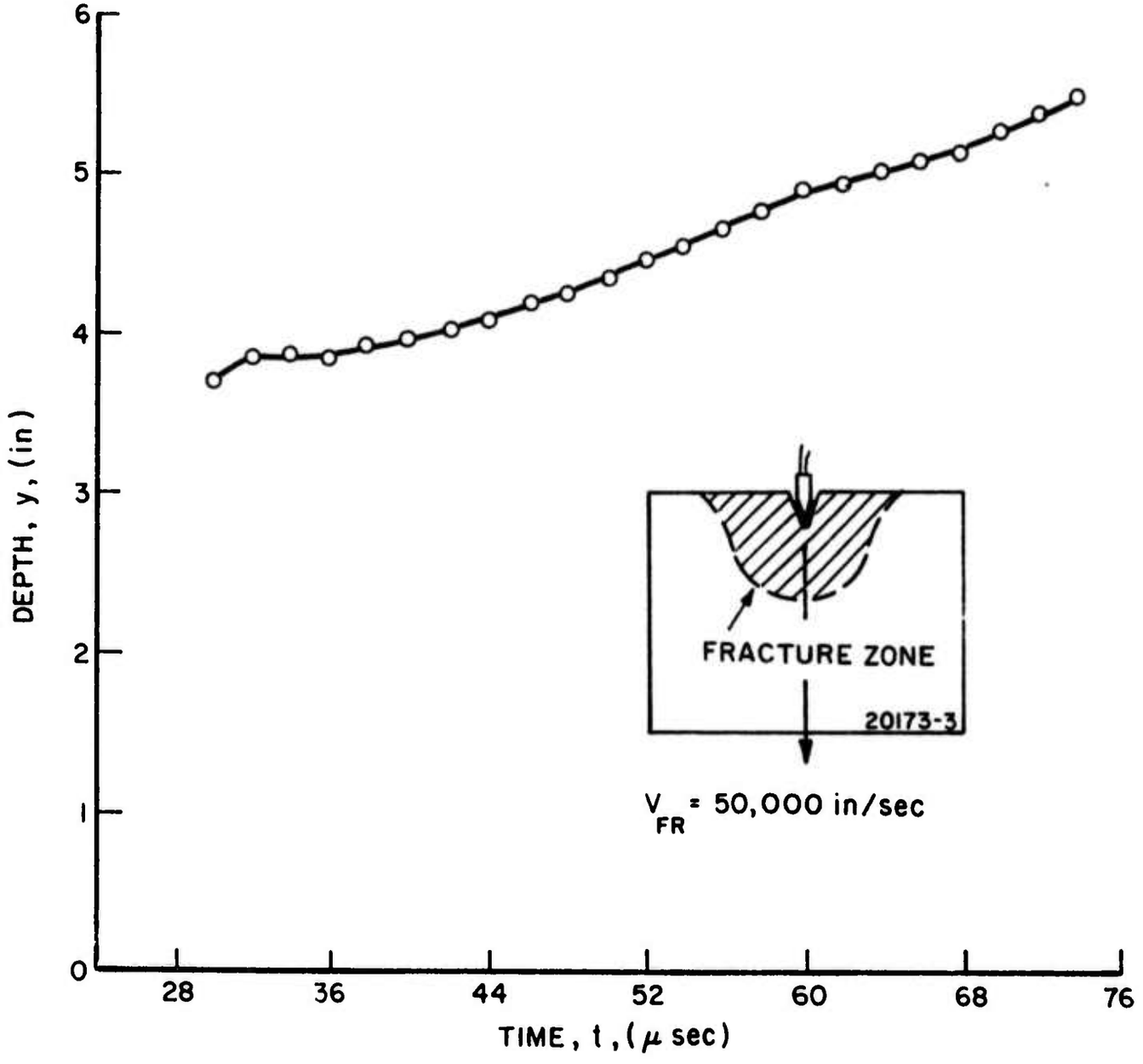

Fig. 36 PROPAGATION OF FRACTURE ZONE BOUNDARY IN MARBLE PLATE LOADED EXPLOSIVELY THROUGH A NOTCH

was measured near the central part of the curve.

Additional marble and granite plates were loaded explosively with an RP-1 detonator and a tetryl pellet placed over a steel wedge inserted in a notch on one edge. Four Argon bombs and Double-X film were used. The camera was operated at a rate of 500,000 frames per second. Figures 37 and 38 show isochromatic fringe patterns in the photoelastic coating around propagating cracks in the marble and granite plates. The crack propagation velocities measured were 38,000 in./sec and 36,000 in./sec for the marble and granite specimens, respectively.

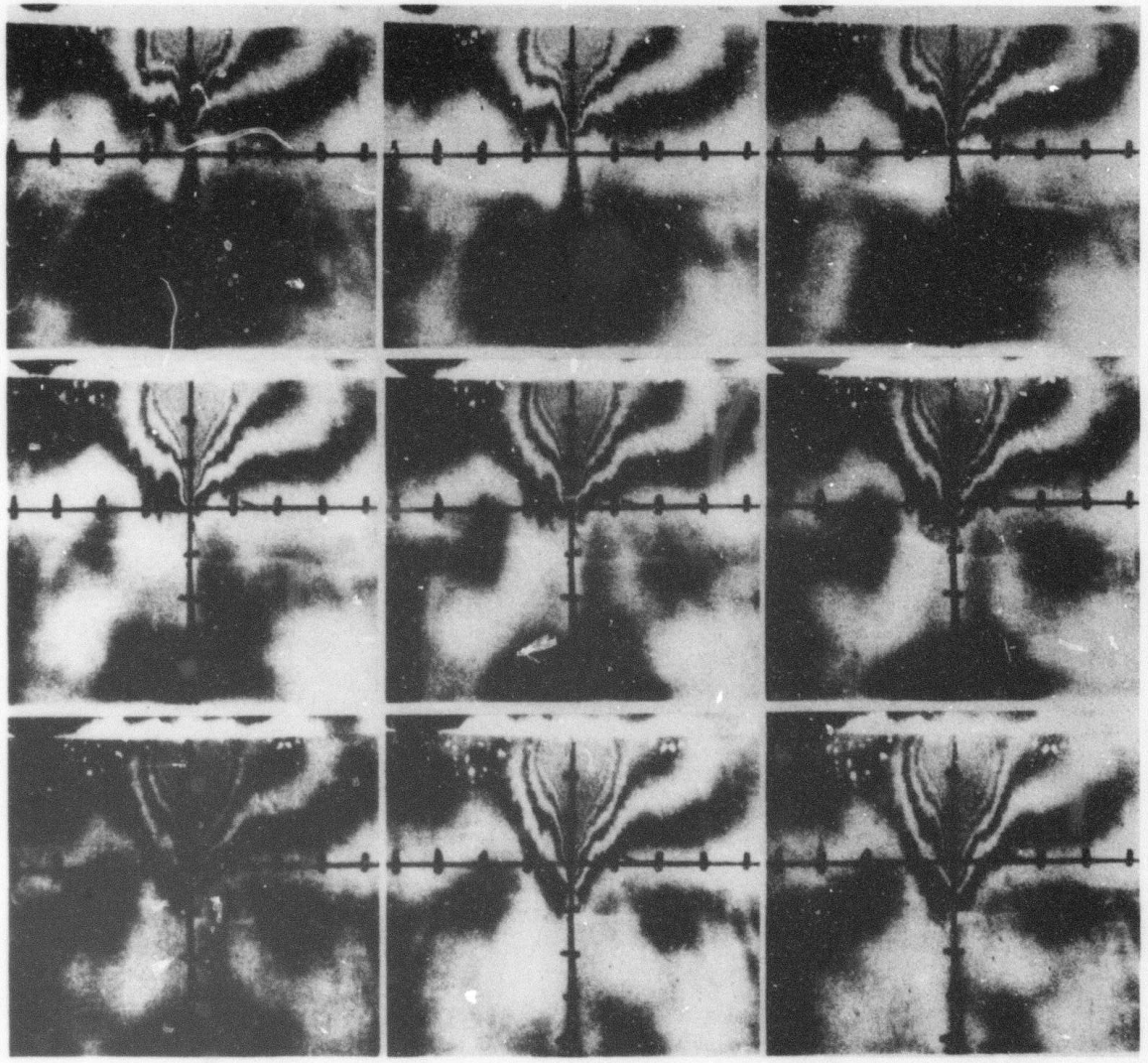

Fig. 37 CRACK PROPAGATION IN MARBLE PLATE LOADED EXPLOSIVELY THROUGH METAL WEDGE IN NOTCH (FRAMES SHOWN ARE AT 4 μ SEC INTERVALS; SPECIMEN 31573-3)

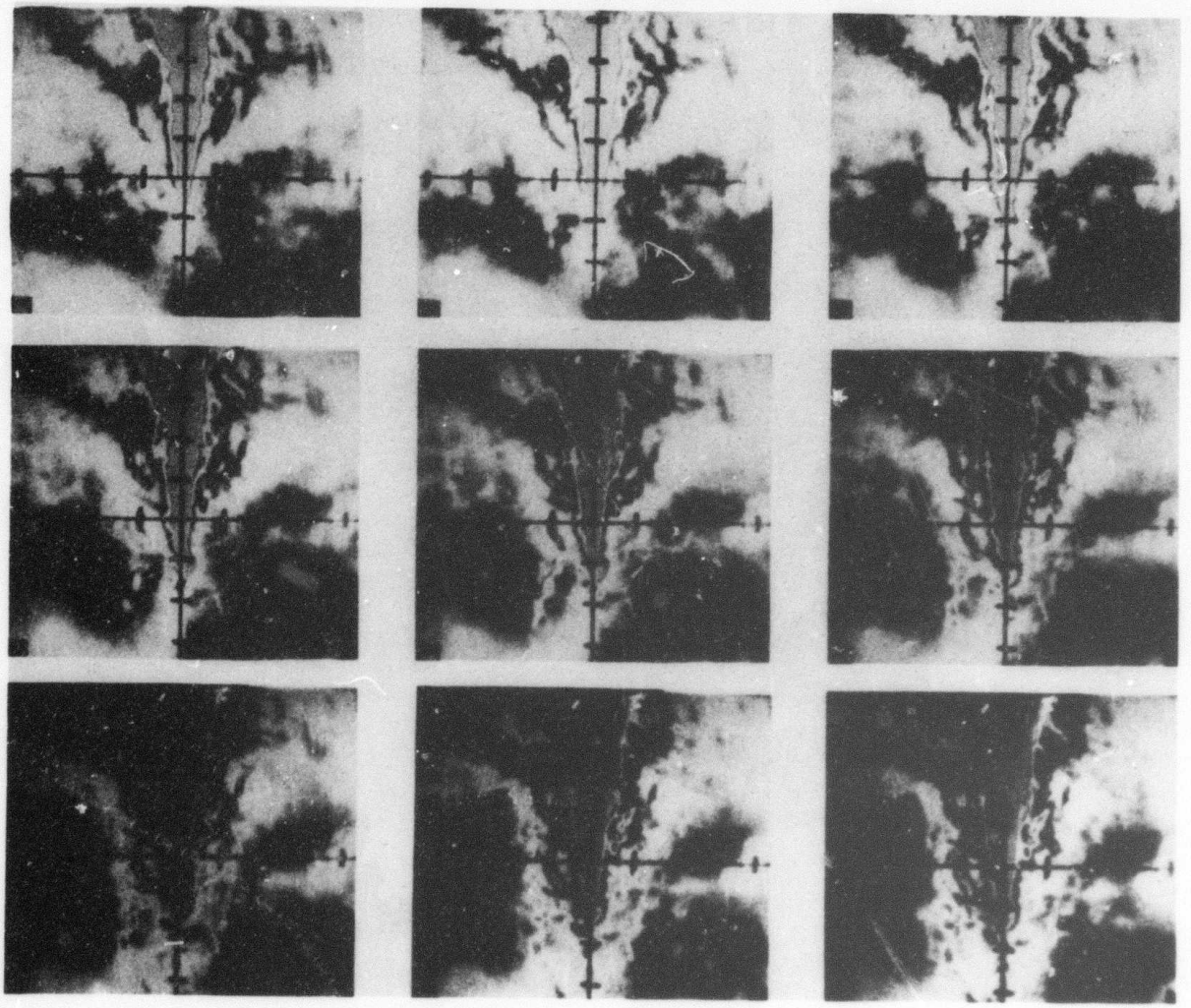

Fig. 38 CRACK PROPAGATION IN GRANITE PLATE LOADED EXPLOSIVELY THROUGH METAL WEDGE IN NOTCH (FRAMES SHOWN ARE AT 4 μ SEC INTERVALS; SPECIMEN: 31573-2)

7.0 SUMMARY AND DISCUSSION

Experimental stress analysis techniques, such as dynamic photoelasticity, moiré and photoelastic coatings were used to study wave and fracture propagation in rock and rocklike media. Materials used in this investigation were transparent rocklike birefringent materials such as Columbia Resin CR-39, Plexiglas and Homalite-100 and two rock materials, namely, Vermont Marble and Cold Spring Granite.

The transparent birefringent specimens were loaded with explosive charges at an interior point and the isochromatic fringe patterns and crack propagation were recorded with a Cranz-Schardin multiple spark camera operating at a rate of 200,000 frames per second. The photographic records obtained were analyzed to determine dilatational wave, shear wave and crack propagation velocities. Some of the results are summarized in Table 2. In the case of the brittle CR-39 material, it was possible to measure crack propagation velocities up to half the measured shear wave velocity, which represents the theoretical limit for fracture propagation. No fracture propagation was observed in Plexiglas and limited fracture was observed in Homalite-100. The crack propagation velocity measured in the latter was only 0.273 times the shear wave velocity, far below the theoretically predicted limiting velocity.

Marble and granite plates were loaded explosively on one edge and isochromatic fringe patterns on bonded photoelastic coatings and moiré fringe patterns were recorded with a Beckman and Whitley camera operating at rates from 250,000 to 1,000,000 frames per second.

Table 2

WAVE AND FRACTURE PROPAGATION IN ROCK AND ROCKLIKE MATERIALS

Material	Measured Dilatational Plate Velocity, c_L, (in./sec)	Shear Wave Velocity c_s (in./sec)		Highest Measured Fracture Propagation Velocity, v_{fr}, in./sec	Velocity Ratio v_{fr}/c_s	
		Measured	Calculated		Measured	Theoretical Limit Value
CR-39	77,750	40,300	44,300	20,500	0.508	0.50
Plexiglas	96,000	53,700	54,600	-	-	-
Homalite-100	89,000	49,500	50,500	13,500	0.273	0.50
Marble	160,000	100,000	98,000	50,000	0.500	0.50
Granite	182,000	-	111,500	36,000	0.323	0.50

Dilatational, shear and Rayleigh wave velocities were measured in marble. Some of the results are tabulated in Table 2. The measured shear wave velocity was almost identical to the one computed from the measured dilatational wave velocity and Poisson's ratio of the material. The characteristics of the propagating pulse were studied. The primary leading part of the pulse is compressive and shows appreciable attenuation but not much noticeable dispersion. The attenuation observed was separated into its geometric and material components. The coefficient of material attenuation in marble was found to be $k = 0.101$ which corresponds to a loss tangent of $\tan \delta = 0.096$.

Transient displacement and strain distributions were determined from the moiré fringe patterns. It was shown that the trailing end of the propagating pulse becomes tensile, thus likely to induce widespread tensile fracture. The dilatational wave propagation velocity was also measured in granite, which also exhibited appreciable attenuation.

To study fracture propagation marble and granite plates were loaded explosively through a notch on one edge. The crack propagation velocities measured were relatively low, below the limiting theoretical values. Crack propagation velocities of 38,000 in./sec and 36,000 in./sec were determined for marble and granite, respectively. The corresponding theoretical terminal velocities are 50,000 and 56,000 in./sec. In the case of one marble specimen loaded with a heavy explosive inside the notch, the propagation velocity of the fracture zone was measured to be 50,000 in./sec. It seems that terminal fracture velocities in rock can be achieved if the pulse is sufficiently intense. The high material and geometric attenuation tends to weaken the propagating pulse and reduce the fracture propagation.

The experimental investigation conducted and described above was of a fundamental nature, aimed at providing a better understanding of the rapid excavation process by explosives. The primary input of an explosive in a rock mass is a compressive pulse traveling with the dilatational wave velocity. The geometric attenuation of such a pulse is very rapid in three-dimensional space, the pulse amplitude varying inversely with the distance from the explosive source. This fact, coupled with the high compressive strength of rock, tends to limit compressive fracturing in the immediate vicinity of the explosive source. However, high speed explosives tend to produce short compressive pulses followed by tensile trailing pulses, as evidenced in the model studies described in this report. The resulting tensile stresses, even though they are of relatively low magnitude, tend to produce more extensive tensile fracture after passage of the pulse, because of the much lower tensile strength of rock.

Tensile rock fracture also results when the primary compressive pulse interacts with preexisting cavities or flaws in the rock mass and when it is reflected as a tensile pulse from a free surface. It is conceivable that the efficiency of explosive excavation could be enhanced by preinducing such cavities or flaws with prior smaller explosives properly spaced and timed.

Multiple explosives suitably timed and spaced can also be used to produce pulses interfering constructively in specified regions of the rock mass, thus producing the maximum fracture for a given total amount of explosive.

Multiple-explosive drilling in rock is a common practice. Systems have been used whereby explosive charges are delivered to the bottom of a well at a steady rate and detonated sequencially while at the same time flushing up the fractured rock chips. A variation of this general approach has been developed recently whereby the explosive charge consists of a series of smaller conical charges aimed in different directions away from the center.[29] This device thus sends out a series of small jets into

the rock in a conical pattern. It is claimed that this system can drill more rock per unit of explosive than previously used systems.

Further developments of this nature can definitely benefit from fundamental laboratory experiments such as described here. Knowledge of the dynamic rock properties and the pulse propagation and attenuation characteristics of the explosive would help in properly designing a series of multiple explosions for maximum efficiency. Further experimental laboratory work with rock specimens is recommended. High-speed photographic techniques can be improved further to record photoelastic and moiré fringe patterns for a more detailed analysis of experimental results. Means for inducing crack propagation at near the theoretical limiting velocity must be explored. The effects of multiple explosive loadings must be studied to determine the optimum spacing and timing of these explosives.

REFERENCES

1. Rapid Excavation, National Academy of Sciences, Washington, D. C., Publication 1690, 1968.

2. Kolsky, H., Stress Waves in Solids, Clarendon Press, 1953.

3. Bieniawski, Z. T., "Fracture Dynamics of Rock," Intern. J. of Fracture Mech., Vol. 4, No. 4, Dec. 1968, pp. 415-430.

4. Ricketts, T. E. and Goldsmith, W., "Dynamic Properties of Rocks and Composite Structural Materials," Int. Journal Rock Mech. Min. Scie., Vol. 7, No. 3, 1970, pp. 315-335.

5. Griffith, A. A., "The Phenomena of Rupture and Flow in Solids," Phil. Trans. of the Royal Soc. of London, Series A, Vol. 221, 1921, pp. 163-197.

6. McClintock, F. A. and Walsh, J. B., "Friction on Griffith Cracks in Rock Under Pressure," Int. Congress on Applied Mech., Berkeley, Calif., 1962.

7. Hoek, E., "Rock Fracture Around Mine Excavations," Proc. 4th Intern. Conf. on Strata Control and Rock Mech., May 4-8, 1964, Henry Crumb School of Mines, Columbia Univ., New York, N. Y.

8. Irwin, G. R., "Fracture," Structural Mechanics, ed. by Goodier and Hoff, Pergamon Press, 1960, pp. 557-592.

9. Yoffe, E. H., "The Moving Griffith Crack," Phil. Mag., Vol. 42, 1951, p. 739.

10. Roberts, D. K. and Wells, A. A., "The Velocity of Brittle Fracture," Engineering, Vol. 178, 1954, p. 820.

11. Baker, B. R., "Dynamic Stresses Created by a Moving Crack," J. Applied Mechanics, Vol. 29, 1962, p. 449.

12. Wells, A. A. and Post, D., "The Dynamic Stress Distribution Surrounding a Running Crack - A Photoelastic Analysis," Proc. SESA, Vol. 16, 1958, p. 69.

13. Schardin, H., Fracture, ed. by Averbach, et al., Wiley, New York, 1959, pp. 297-330.

14. Hoek, E. and Bieniawski, Z. T., "Brittle Fracture Propagation in Rock Under Compression," Intl. Jour. Fract. Mech., Vol. 1, No. 3, Sept. 1965, pp. 137-155.

15. Bieniawski, Z. T., "The Phenomenon of Terminal Velocity in Rock," Rock Mech. and Eng'r. Geol., 1968.

REFERENCES (Cont'd.)

16. Bieniawski, Z. T., "An Application of High-Speed Photography to the Determination of Fracture Velocity in Rock," Proc. 8th Int'l. Cong. High-Speed Photography, 1968, pp. 440-443.

17. Persson, A., "High-Speed Photography of Full-Model Rock Blasting," Proc. 9th Int'l. Cong. on High-Speed Photography, Denver, 1970.

18. Field, J. and Ladegaard-Pedersen, A., "The Importance of the Reflected Shock Wave in Rock Blasting," Swedish Detonic Res. Foundation Report DL 1969:7.

19. Denkhaus, H. G., "The Application of the Mathematical Theory of Elasticity to Problems of Stress in Hard Rock at Great Depth," Assoc. Mine Managers of S. Africa, Papers and Discussions, Vol. 1958-59, Sept. 1958, pp. 271-310.

20. Daniel, I. M. and Rowlands, R. E., "Deformation and Fracture Around Lined and Unlined Cylindrical Cavities in Rocks," Experimental Mechanics, Vol. 11, Oct. 1971, pp. 473-480.

21. Poncelet, E. F., Metal Technology, Vol. 11, Tech. Publ. No. 1684, April 1944.

22. Abbott, B. W. and Cornish, R. H., "A Stress Wave Technique for Determining the Tensile Strength of Brittle Materials," Experimental Mechanics, Vol. 5, May 1965, pp. 148-153.

23. Flynn, P. D., "Dynamic Photoelasticity," Trans. Inst. Soc. America, 5(1), 1966, pp. 65-73.

24. Cole, A. A., Quinlan, J. F. and Zandman, F., "The Use of High-Speed Photography and Photoelastic Coatings for the Determination of Dynamic Strains," Proc. 5th Int'l. Cong. on High-Speed Photography, 1962, pp. 250-261.

25. deGraf, J.G.A., "Investigation of Brittle Fracture in Steel by Means of Ultra-High Speed Photography, J. Appl. Optics, 3(11), 1964, pp. 1223-1229.

26. Rowlands, R. E., Taylor, C. E. and Daniel, I. M., "Ultrahigh-Speed Framing Photography Employing a Multiply-Pulsed Ruby Laser and a Smear-Type Camera," Proc. 8th Int'l. Congress High-Speed Photography, ed. by N. R. Nilsson and L. Hogberg, Stockholm, pp. 275-280, 1968.

REFERENCES (Cont'd.)

27. Rowlands, R. E. and Taylor, C. E., "Pulsed Laser High-Speed Photography," Proc. Int'l. Cong. on Instrumentation (IEEE), Polytechnic Institute of Brooklyn, 1969, pp. 145-159.

28. Flynn, P. D., "Photoelastic Studies of Dynamic Stresses in High Modulus Materials," Soc. of Motion Picture and Television Eng., Inc., Reprint No. 99-21, presented at 99th Technical Conference, May 1-6, 1966.

29. "Rock Mechanics and Rapid Excavation Using Explosives," AAI Corp., Weapons and Aero Systems Division, Baltimore, Maryland, Semiannual Report for Bureau of Mines, Twin Cities, Minnesota, Contract No. HO220017, August 1972.